

Fast-Rolling Relaxion

Masahiro Ibe,^{1,2} Yutaro Shoji,³ and Motoo Suzuki^{1,2}

¹*Institute for Cosmic Ray Research (ICRR),*

The University of Tokyo, Kashiwa, Chiba 277-8582, Japan

²*Kavli IPMU (WPI), UTIAS The University of Tokyo, Kashiwa, Chiba 277-8583, Japan*

³*Kobayashi-Maskawa Institute for the Origin of Particles and the Universe,*

Nagoya University, Nagoya 464-8602, Japan

Abstract

We discuss new mechanisms to stop the relaxion field during inflation. They can be realized in a generic model, including the original model but in a quite different parameter region. We consider a *fast-rolling* relaxion field, which can go over the bumps created by QCD-like dynamics. Then, in one of the mechanisms, we stop it with a parametric resonance of the Higgs field. The mechanisms are free from a super-Planckian field excursion or a gigantic number of e -folds of inflation. The relaxion has a mass around the weak scale and mixes with the Higgs boson, which enhances the testability of our mechanisms.

I. INTRODUCTION

The succession of null results of new physics search at the Large Hadron Collider (LHC) might imply that the energy scale of new physics is higher than the TeV scale. If this is the case, the Higgs mass parameter seems to be severely fine-tuned since it is highly sensitive to the energy scale of new physics. The gap between the two scales is worth considering since a mechanism might reside behind it.

Among various possibilities, it is interesting that the electroweak (EW) scale is determined dynamically with a new field, called the relaxion [1]. It scans the Higgs mass squared during inflation, rolling down a linear potential. After the relaxion passes the *critical point*, where the Higgs mass squared becomes zero, the Higgs field develops a vacuum expectation value (VEV). It triggers a back-reaction and the relaxion stops around the critical point. Since the Higgs mass squared is determined independently of its initial value, we can naturally explain the gap between the two scales. The back-reaction can be implemented by using an axion-like coupling of the relaxion to strong dynamics, which generates bumps that depend on the value of the Higgs field. Although the idea is in an early stage of development, there are already a number of papers discussing its phenomenology or its variants [2–38].

In the original model, the relaxion is assumed to slow-roll so that it stops immediately after the bumps match the slope of the linear potential. Since the potential barrier is very low at that point, the first selected vacuum quickly decays or hops into the lower vacuum through quantum tunneling or the Hubble fluctuations. The relaxion continues to decay, or hop for the first bumps, to lower vacua until it finds a vacuum whose lifetime is much longer than the age of the universe. This process, however, requires a gigantic number of e -folds since the Hubble volume during inflation is very small. To be consistent with the age of the universe, the bubble nucleation rate in the final vacuum, γ , should satisfy

$$\gamma \ll H_0^4, \quad (1)$$

with H_0 being the Hubble constant of the current universe. For such a vacuum to decay during the inflation era, we need a gigantic number of e -folds, \mathcal{N}_e , as

$$\mathcal{N}_e > \frac{H^4}{\gamma} \gg \left(\frac{H}{H_0} \right)^4, \quad (2)$$

with H being the Hubble constant during inflation. It easily exceeds 10^{150} even with a low scale inflation, which causes problems in the inflation sector. If one considers slow-roll inflation during the relaxation, for example, the number of e -folds is expected to be lower than 10^{24} to avoid fine-tuning problems [6, 39–42]. Alternatively, one may assume eternal inflation during the relaxation. It, however, induces multiverse, which obscures the virtue of the relaxion mechanism.¹

A simple solution to the above problem is to violate one of the slow-roll conditions and allow the relaxion to fly over the bumps with its kinetic energy.² In compensation, we need another mechanism to stop the relaxion at a desired position. Several alternative mechanisms have already been proposed. For example, [5, 7–11] use particle production and [4] uses potential instability to stop the relaxion. Such mechanisms can also avoid a super-Planckian excursion of the relaxion, which is often troublesome when one UV-completes the model. In addition, it also reduces the number of e -folds during the slow-rolling phase.

In this paper, we discuss two stopping mechanisms, which can be realized without extending the original model. One is to use Higgs coherent oscillation caused by a parametric resonance, and the other is rather close to the original mechanism. In this paper, we focus on the former one and provide a detailed analysis. For the latter, we only sketch the idea and give an example in the Appendix C. In both mechanisms, the relaxion mass lies around the weak scale and mixes with the Higgs boson, which enhances the testability of these mechanisms. In addition, classical rolling always dominates over quantum fluctuations during the relaxation. Thus, the Higgs VEV is determined almost identically over different Hubble patches, which cures the *oddity* raised in the original model [1].

This paper is organized as follows. In Section II, we briefly review the original relaxion model with QCD-like dynamics, which we use throughout this paper. An overview of our first mechanism is given in Section III. Since we use a parametric resonance to stop the relaxion, we explain it in Section IV. Then, we discuss resonant particle production in Section V. After a short review of a vacuum decay rate in Section VI, we summarize theoretical and experimental constraints in Section VII. Then, we show an example parameter region in Section VIII. In Section IX, we discuss how an appropriate potential of the relaxion can be

¹ It has been also argued that eternal inflation is generically incompatible with the (refined) de Sitter swampland conjecture [43–45]. The hilltop eternal inflation is marginally consistent with the refined de Sitter swampland conjecture, but the Hubble constant naturally lies around the Planck scale in such a case.

² Another solution is make $\epsilon = 0$ after the relaxation, which is discussed in the context of solving the strong CP problem in the QCD relaxion model [1].

obtained, identifying it with a pseudo Nambu-Goldstone boson (NGB). We also discuss the origin of the fast-rolling in the latter part of the section. The final section is devoted to our conclusions.

II. MODEL

We review the original non-QCD relaxion model [1] in this section.

The Lagrangian is defined as

$$\mathcal{L} = \sqrt{-g} \left[\frac{1}{2}(\partial X)^2 + |D\Phi|^2 - V(\Phi, X) \right] + \mathcal{L}_{\text{SM}} , \quad (3)$$

where

$$V(\Phi, X) = (M^2 - \epsilon X)|\Phi|^2 - r\epsilon M^2 X + \Lambda^4(|\Phi|^2) \cos\left(\frac{X}{f}\right) + \frac{\lambda}{4}|\Phi|^4 , \quad (4)$$

and \mathcal{L}_{SM} is the SM Lagrangian without the Higgs potential. Here, we denote the relaxion field and the Higgs doublet as X and Φ , respectively. The Higgs quartic coupling, λ , is almost the same as that in the SM, while the Higgs mass, M^2 , is assumed to lie around a new physics scale. To relax the hierarchy between the two scales, we introduce a coupling between the Higgs boson and the relaxion, where the small coupling constant, ϵ , is technically natural (see Section IX). Since ϵ breaks the shift symmetry of the relaxion, we expect a tadpole term of the relaxion with $|r| \gtrsim 1/16\pi^2$. We assume M^2 , ϵ and r are positive. We have another source of the shift symmetry breaking due to non-QCD strong dynamics, which we assume to have the form of

$$\Lambda^4(|\Phi|^2) = \frac{\Lambda_0^4}{2} + \Lambda_h^2 |\Phi|^2 . \quad (5)$$

The simplest example of the new strong sector is given in [1], where we introduce new light fermions having the same SM charges as a right handed neutrino, N and N^c , and new heavy fermions having the same SM charges as a lepton doublet, L and L^c .³ They are charged under a new $SU(3)$ group, whose field strength is denoted as $G_{\mu\nu}^a$. The relevant part of the Lagrangian is given by

$$\mathcal{L}_{\text{UV}} = \mathcal{L}_{\text{kin.}} - \frac{1}{32\pi^2} \frac{X}{f} G_{\mu\nu}^a \tilde{G}^{a\mu\nu} + m_L L L^c + m_N N N^c + (y\Phi L N^c + \tilde{y}\Phi^\dagger L^c N + h.c.) , \quad (6)$$

³ In this paper, all the fermions without a dagger represent left-handed Weyl fermions.

where f is a decay constant of the relaxion, y and \tilde{y} are Yukawa couplings, and \mathcal{L}_{kin} includes the kinetic terms. After integrating out L , the mass of N is given by

$$m_N^{(\text{eff})} \simeq m_N - \frac{y\tilde{y}}{8\pi^2} m_L \ln \frac{M^2}{m_L^2} - \frac{y\tilde{y}}{m_L} |\Phi|^2, \quad (7)$$

at the one-loop level. If $m_N^{(\text{eff})}$ is smaller than the dynamical scale of the new strong dynamics, Λ_c , NN^c condensates and generates

$$\Lambda_0^4 \simeq 2 \left(m_N - \frac{y\tilde{y}}{8\pi^2} m_L \ln \frac{M^2}{m_L^2} \right) \Lambda_c^3, \quad (8)$$

$$\Lambda_h^2 \simeq -\frac{y\tilde{y}}{m_L} \Lambda_c^3. \quad (9)$$

In this paper, we assume that Λ_c is smaller than m_L .

III. MECHANISM

In this section, we give an overview of our first mechanism. The main difference from the original model is that the relaxion does not slow-roll due to

$$H \lesssim \left| \frac{\ddot{X}}{\dot{X}} \right|, \quad (10)$$

where H is the Hubble constant during inflation and the dot indicates the time derivative. In this case, the original stopping mechanism does not work since the kinetic energy of the relaxion is not negligible. Instead, we use the following mechanism.

1. The initial Higgs mass squared is assumed to be positive at the onset of relaxation. The relaxion rolls down the potential with its terminal velocity until the Higgs mass squared becomes smaller than Λ_h^2 .
2. When the Higgs mass squared decreases down to a certain positive value, the Higgs field starts to oscillate homogeneously due to a parametric resonance, which is explained in the next section. The amplitude of the oscillation grows *gradually* as the Higgs mass becomes smaller.
3. The Higgs oscillation is then fed back to the relaxion roll in the following ways; (i) the

height of the bumps of the relaxion potential oscillates, (ii) the relaxion slows down due to the additional Hubble friction acting on the Higgs field. Since they hinder the roll, the relaxion eventually hits a bump and bounces back.

4. Just after the bounce of the relaxion, the Higgs field finds its mass is negative due to the negative contribution from the second term in Eq. (5), and develops a VEV. The sudden development of the Higgs VEV plays a role of an anchor, which secures the relaxion in a potential well between the bumps.
5. Once the anchor bites, the Higgs field can not return to the symmetric point due to the Hubble friction, and the oscillation around the VEV dumps quickly. It finalizes the relaxation.

It should be noticed that the Higgs mass squared is typically *positive* when the relaxion stops unlike in the original mechanism. However, it does not matter since the Higgs mass squared has been reduced to a value smaller than Λ_h^2 , and the negative Higgs mass squared is provided by $\Lambda_h^2 \cos(X/f)$.

IV. EDGE SOLUTION

In this section, we show the behavior of the Higgs field around the critical point, which triggers our stopping mechanism.

Before going into discussion, let us summarize the equations of motion for the homogeneous modes of the relaxion and the Higgs field, which are denoted by $\bar{X}(t)$ and $\bar{h}(t)$, respectively. They are given by

$$\ddot{\bar{X}} + 3H\dot{\bar{X}} = \epsilon \left(rM^2 + \frac{\bar{h}^2}{2} \right) + \frac{\Lambda_0^4 + \Lambda_h^2 \bar{h}^2}{2f} \sin \frac{\bar{X}}{f}, \quad (11)$$

$$\ddot{\bar{h}} + 3H\dot{\bar{h}} = -(M^2 - \epsilon\bar{X})\bar{h} - \frac{\lambda}{4}\bar{h}^3 - \Lambda_h^2 \bar{h} \cos \frac{\bar{X}}{f}, \quad (12)$$

where we choose a basis of the Higgs field as

$$\Phi = \frac{1}{\sqrt{2}} \begin{pmatrix} \eta^1 + i\eta^2 \\ h + i\eta^3 \end{pmatrix}. \quad (13)$$

Here, η^a 's are taken so that their expectation values are always zero without loss of generality.

One might think that nothing happens during the roll of the relaxion since the simplest solution to the equations of motion is

$$\bar{X}(t, \mathbf{x}) \simeq \frac{r\epsilon M^2}{3H}(t - t_0) , \quad (14)$$

$$\bar{h}(t, \mathbf{x}) \simeq 0 , \quad (15)$$

with t_0 being a constant. However, it is not always a stable solution and there appears another branch of stable solutions where the oscillation of \bar{h} grows gradually.

A. Simplified System

Let us first see that the solution of (14) and (15) is not stable using a simple differential equation. Plugging Eq. (14) into Eq. (12), one obtains a differential equation that looks like

$$\ddot{y} + (m^2(t) + \Lambda^2 \cos \omega t) y + \frac{\lambda}{4} y^3 = 0 , \quad (16)$$

with $y \sim \bar{h}$ and

$$m^2(t) = m_0^2 - \delta m^2 t . \quad (17)$$

Here, ω , m_0^2 and δm^2 are the constants determined by the model parameters and we have ignored the Hubble friction acting on the Higgs field for simplicity.

A numerical solution to Eq. (16) is shown in the left panel of Fig. 1. The solid blue line corresponds to the solution with

$$\lambda = 0.52, \quad m_0^2 = 4700, \quad \delta m^2 = 470, \quad \Lambda = 60, \quad \omega = 100 , \quad (18)$$

where the unit of scale is arbitrary. The initial conditions of y are irrelevant if it is small enough but non-zero.

We can see that y starts to oscillate around $t \sim 2$ and the amplitude grows gradually afterwards, which shows that the solution described by (14) and (15) is unstable with the above parameter set. We call the solutions that behave like this the *edge solutions* and

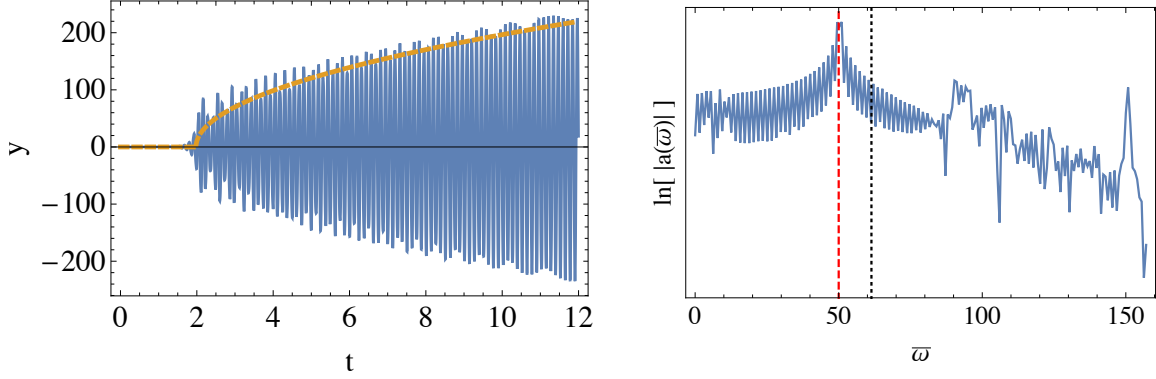


FIG. 1. A solution to Eq. (16) with the parameters given in (18). *Left:* The solid blue line shows the numerical solution and the dashed orange line shows the amplitude obtained with Eq. (27). The solution represents the evolution of the Higgs field in a simplified treatment. *Right:* The coefficients of the Fourier cosine series, $a(\bar{\omega})$, with $\bar{\omega}$ being a frequency of $y(t)$. It is calculated for $8 < t < 12$. The dashed red line indicates $\bar{\omega} = \omega/2$ and the dotted black line indicates $\bar{\omega} = \sqrt{m^2}$.

explain how they are stabilized below.

If we ignore the non-linear term and the time dependence of m^2 in Eq. (16), the equation becomes the so-called Mathieu equation, which exhibits instability for⁴

$$\frac{\omega^2 - 2\Lambda^2}{4} \lesssim m^2 \lesssim \frac{\omega^2 + 2\Lambda^2}{4} . \quad (19)$$

Since m^2 decreases monotonically due to the motion of the relaxion, it enters the above resonance band and y starts to grow exponentially.

The exponential growth, however, stops immediately after the non-linear term in Eq. (16) becomes important. To understand the effect of the non-linear term, let us analyze the differential equation given by

$$\ddot{\tilde{y}}(t) + m^2 \tilde{y}(t) + \frac{\lambda}{4} \tilde{y}^3(t) = 0 , \quad (20)$$

assuming m^2 is constant. A relevant oscillating solution is given by

$$\begin{aligned} \tilde{y}(t) &= \mathcal{A} \operatorname{sn} \left(\sqrt{m^2 + \frac{\lambda}{8} \mathcal{A}^2} t, -\frac{\mathcal{A}^2 \lambda}{8m^2 + \mathcal{A}^2 \lambda} \right) \\ &\simeq \mathcal{A} \sin(\bar{m}(\mathcal{A})t) , \end{aligned} \quad (21)$$

⁴ Here, we consider the first resonance band of the Mathieu equation. We will comment on the effects of the higher resonance bands later.

where $\text{sn}(u, k)$ is the Jacobi elliptic sine function and

$$\overline{m}^2(\mathcal{A}) = \frac{\pi^2(8m^2 + \mathcal{A}^2\lambda)}{32 \left[K \left(-\frac{\mathcal{A}^2\lambda}{8m^2 + \mathcal{A}^2\lambda} \right) \right]^2} \simeq m^2 + \frac{3}{16}\lambda\mathcal{A}^2 . \quad (22)$$

Here, $K(k)$ is the complete elliptic integral of the first kind, which is defined as

$$K(k^2) = \int_0^{2/\pi} \frac{1}{\sqrt{1 - k^2 \sin^2 \theta}} d\theta . \quad (23)$$

It motivates us to approximate the original differential equation as

$$\ddot{Y} + (\overline{m}^2(\mathcal{A}) + \Lambda^2 \cos \omega t) Y = 0 , \quad (24)$$

with \mathcal{A} being the amplitude of the oscillation. Let us describe the behavior of the solution as follows. When \overline{m}^2 enters the resonance band, \mathcal{A} starts to grow exponentially. Since it makes \overline{m}^2 larger, the growth stops immediately. However, since m^2 decreases due to the motion of the relaxation, it re-enters the resonance band and the amplitude grows until \overline{m}^2 gets out of the resonance band. These occur repeatedly and the amplitude is kept around the *edge* of the resonance band.

Let us discuss it more quantitatively and justify the above description. Assuming \overline{m}^2 is a constant, one can construct a solution to Eq. (24) that behaves like

$$Y(t) = e^{\frac{i}{2}\nu\omega t} u(t) , \quad (25)$$

where $u(t)$ is an $\mathcal{O}(1)$ function having a periodicity ω . As discussed in Appendix A, ν can be approximated as

$$\nu \simeq 1 \pm \frac{i}{2} \sqrt{\frac{4\Lambda^4}{\omega^4} \left(1 - \frac{3\Lambda^4}{8\omega^4} \right) - \left(\frac{4\overline{m}^2}{\omega^2} - 1 + \frac{3\Lambda^4}{2\omega^4} \right)^2} , \quad (26)$$

around the first resonance band. When ν has an imaginary part, the amplitude grows exponentially. Assuming \overline{m}^2 is kept around the edge of the resonance band, i.e. $\text{Im}(\nu) \simeq 0$

, we can predict the amplitude as

$$m^2 + \frac{3}{16}\lambda\mathcal{A}^2 \simeq \frac{\omega^2}{4} \left(1 - \frac{3}{2}\frac{\Lambda^4}{\omega^4}\right) + \frac{\Lambda^2}{2} \sqrt{1 - \frac{3}{8}\frac{\Lambda^4}{\omega^4}}. \quad (27)$$

We show the amplitude, \mathcal{A} , determined by Eq. (27) with the dashed orange line in the left panel of Fig. 1. Notice that the time dependence of \mathcal{A} comes from $m^2(t)$. As we can see from the figure, the predicted amplitude agrees well with the numerical solution, supporting our intuitive description.

Another justification comes from the frequency of the amplified mode. Since the real part of ν is one, we expect that the frequency of $y(t)$ peaks around $\omega/2$. In the right panel of Fig. 1, we plot the coefficients of the Fourier cosine series for $8 < t < 12$. It clearly shows that the frequency of the amplified mode is $\omega/2$ as indicated with the red dashed line. For comparison, we show $\sqrt{m^2}$ determined by Eq. (27) with the black dotted line. Notice that m^2 is irrelevant since $-30^2 \lesssim m^2 \lesssim 30^2$ in this interval.

B. Relaxion-Higgs System

The solution obtained in the previous subsection can not be directly used in our analysis since it does not include the Hubble friction and feedback to the relaxion dynamics.

We search for an edge solution, which has the form of

$$\bar{X}(t) \simeq \frac{M^2 - m_\Phi^2}{\epsilon} + f\omega_X t, \quad (28)$$

$$\bar{h}(t) \simeq \mathcal{A}_h \cos\left(\frac{\omega_X}{2}t - \alpha\right), \quad (29)$$

where α , ω_X , m_Φ^2 and \mathcal{A}_h are treated as constants for $|t| \ll |m_\Phi^2/(\epsilon f\omega_X)|$. The time dependence of these constants will be taken into account by shifting m_Φ^2 so that it cancels the last term of Eq. (28). In Appendix B, we determine α as

$$\sin 2\alpha \simeq -\frac{3H\omega_X}{\Lambda_h^2}, \quad \cos 2\alpha < 0, \quad (30)$$

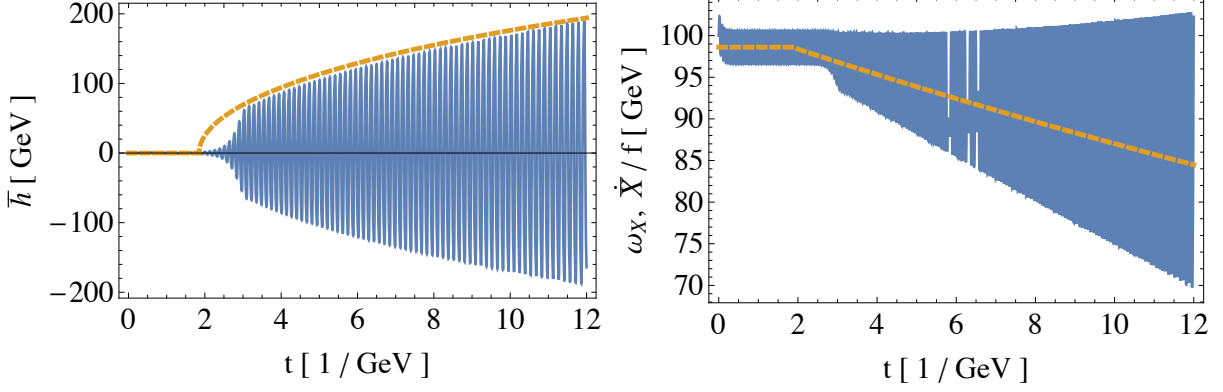


FIG. 2. A comparison between a numerical solution to Eqs. (11) and (12) and the analytic result given in Eqs. (31) and (32). *Left:* The blue line shows \bar{h} and the orange line shows \mathcal{A}_h . *Right:* The blue line shows \dot{X}/f and the orange line shows ω_X .

and obtain relations among ω_X , m_Φ^2 and \mathcal{A}_h as

$$m_\Phi^2 + \frac{3\lambda}{16}\mathcal{A}_h^2 \simeq \frac{\omega_X^2}{4} + \frac{\Lambda_h^2}{2} - \frac{\Lambda_h^2(32\Lambda_0^4 + 17\Lambda_h^2\mathcal{A}_h^2)}{128f^2\omega_X^2} - \frac{(8\Lambda_h^2 - 3\lambda\mathcal{A}_h^2)(8\Lambda_h^2 - \lambda\mathcal{A}_h^2)}{512\omega_X^2} - \frac{9\omega_X^2}{4\Lambda_h^2}H^2, \quad (31)$$

$$\omega_X \simeq \frac{r\epsilon M^2}{3Hf} - \frac{\mathcal{A}_h^2\omega_X}{8f^2} - \frac{\lambda\mathcal{A}_h^4}{128f^2\omega_X} + \frac{3\mathcal{A}_h^2\omega_X^3}{16f^2\Lambda_h^4}H^2, \quad (32)$$

ignoring $\mathcal{O}(1/\omega_X^3)$, $\mathcal{O}(H^2/\omega_X)$ and $\mathcal{O}(H^3)$ corrections. It should be noted that the Higgs oscillation does not grow due to the Hubble friction in the case of $3H\omega_X/\Lambda_h^2 \gtrsim 1$.

In Fig. 2, we compare a numerical solution to Eqs. (11) and (12) with the analytic results given in Eqs. (31) and (32). The left panel shows \bar{h} (blue) and \mathcal{A}_h (orange), and the right panel shows \dot{X}/f (blue) and ω_X (orange). We take

$$\begin{aligned} \lambda &= 0.52, \quad H = 5 \text{ GeV}, \quad \Lambda_0 = \Lambda_h = 60 \text{ GeV}, \quad \epsilon = 0.026 \text{ GeV}, \quad r = 0.01, \\ f &= 180 \text{ GeV}, \quad M = 32 \text{ TeV}. \end{aligned} \quad (33)$$

At $t = 0$, we set $M^2 - \epsilon\bar{X} \simeq 4700 \text{ GeV}^2$ and take $\dot{\bar{X}}$ around the terminal velocity. To mimic quantum fluctuations of \bar{h} , we take⁵ $\bar{h} \simeq H/(2\pi)$ at $t = 0$ and switch off the Hubble friction when $|\bar{h}|$ is smaller than $H/(2\pi)$. As we can see from the left panel, the amplitude is well approximated by Eqs. (31) and (32) once the amplitude reaches the dashed line. From the

⁵ The behavior of the solution is almost independent of this value.

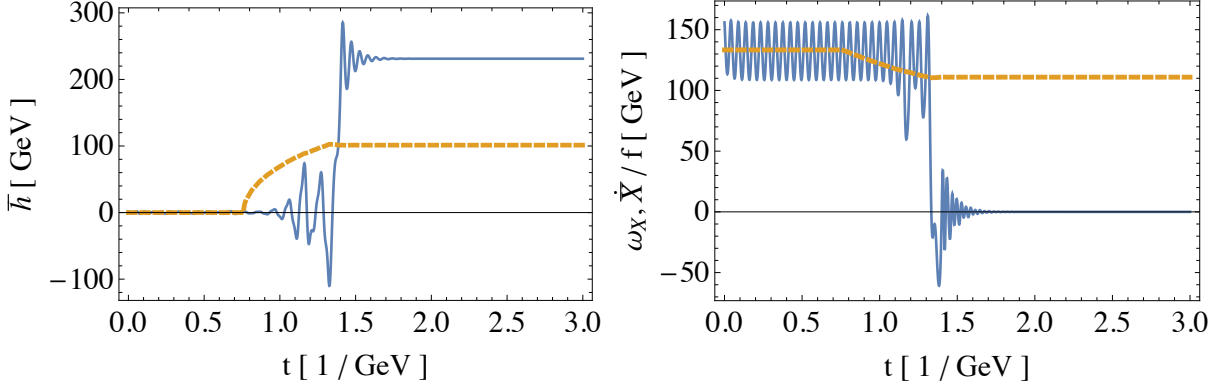


FIG. 3. The same figures as in Fig. 2 with the parameter set given in Eq. (34).

right panel, we see that the predicted ω_X roughly reproduces the time average of $\dot{\bar{X}}/f$.

In Fig. 3, we show another example where the relaxion hits a bump and gets trapped in a potential well. Here, we take the following parameters.

$$\begin{aligned} \lambda = 0.52, \quad H = 10 \text{ GeV}, \quad \Lambda_0 = 80 \text{ GeV}, \quad \Lambda_h = 100 \text{ GeV}, \quad \epsilon = 0.8 \text{ GeV}, \quad r = 0.001, \\ f = 80 \text{ GeV}, \quad M = 20 \text{ TeV}. \end{aligned} \quad (34)$$

We set $M^2 - \epsilon \bar{X} \simeq 13800 \text{ GeV}^2$ at $t = 0$. As the figure shows, the relaxion hits a bump at around $t \sim 1.3 \text{ GeV}^{-1}$ and the Higgs field quickly develops a VEV just like an anchor, securing the relaxion. After the relaxation, we have $M^2 - \epsilon \bar{X} \simeq 3000 \text{ GeV}^2$ and the negative Higgs mass squared is provided by $\Lambda_h^2 \cos(\bar{X}/f)$.

Finally, let us comment on other resonance bands. So far, we have used the first resonance band for the edge solution, but similar solutions with the second and higher resonance bands should also exist. One could eliminate them by taking a large enough Hubble constant since they are much weaker than the first one. However, it is not necessary because the Higgs field does not develop its VEV after the relaxion hits a bump. Since the anchor does not bite, the relaxion continues to roll.

V. SUPPRESSION OF RESONANT PARTICLE PRODUCTION

In the previous section, we have analyzed the homogeneous modes of the relaxion and the Higgs field. However, in field theory, we have to take into account the dynamics of

inhomogeneous modes as well. In particular, resonant particle production can affect our mechanism in the following ways.

- Thermal bath induces thermal potential.
- Thermal bath behaves like friction for the Higgs field and the relaxion.
- Large fluctuations of the relaxion may average out the bumps.
- Increase of the temperature may cause phase transition and erase the bumps.

Although they do not always spoil our mechanism, we seek a parameter space where the particle production is suppressed to keep our analysis as simple as possible.

Let us start with classical field theory. We separate the fields into the homogeneous modes and fluctuations around them as

$$X(x, t) = \bar{X}(t) + \varphi(x) , \quad (35)$$

$$h(x, t) = \bar{h}(t) + \chi(x) . \quad (36)$$

In the Fourier space, the fluctuations are expanded as

$$\varphi(x) = \int \frac{d^3k}{(2\pi)^3} \varphi_{\mathbf{k}}(t) e^{i\mathbf{k}\cdot\mathbf{x}} , \quad (37)$$

$$\chi(x) = \int \frac{d^3k}{(2\pi)^3} \chi_{\mathbf{k}}(t) e^{i\mathbf{k}\cdot\mathbf{x}} . \quad (38)$$

For small fluctuations, they satisfy

$$\ddot{\varphi}_{\mathbf{k}} + 3H\dot{\varphi}_{\mathbf{k}} + \left(m_{\varphi}^2 + \frac{|\mathbf{k}|^2}{a^2(t)} \right) \varphi_{\mathbf{k}} + \delta m_{\varphi}^2 \varphi_{\mathbf{k}} + \delta m_{\text{mix}}^2 \chi_{\mathbf{k}} = 0 , \quad (39)$$

$$\ddot{\chi}_{\mathbf{k}} + 3H\dot{\chi}_{\mathbf{k}} + \left(m_{\chi}^2 + \frac{|\mathbf{k}|^2}{a^2(t)} \right) \chi_{\mathbf{k}} + \delta m_{\chi}^2 \chi_{\mathbf{k}} + \delta m_{\text{mix}}^2 \varphi_{\mathbf{k}} = 0 , \quad (40)$$

where⁶

$$m_\varphi^2 \simeq \frac{\Lambda_h^2 \mathcal{A}_h^2}{8f^2} , \quad (41)$$

$$\delta m_\varphi^2 \simeq -\frac{2\Lambda_0^4 + \Lambda_h^2 \mathcal{A}_h^2}{4f^2} \cos \omega_X t + \frac{\Lambda_h^2 \mathcal{A}_h^2}{8f^2} \cos 2\omega_X t , \quad (42)$$

$$m_\chi^2 \simeq m_\Phi^2 + \frac{3}{8} \lambda \mathcal{A}_h^2 , \quad (43)$$

$$\delta m_\chi^2 \simeq \left(\Lambda_h^2 - \frac{3\lambda}{8} \mathcal{A}_h^2 \right) \cos \omega_X t , \quad (44)$$

$$\delta m_{\text{mix}}^2 \simeq -\frac{\Lambda_h^2 \mathcal{A}_h}{2f} \left(\cos \frac{\omega_X}{2} t - \cos \frac{3\omega_X}{2} t \right) . \quad (45)$$

with $a(t) = e^{Ht}$ being the scale factor. Here, we substituted the edge solution given by Eqs. (28) and (29). We have ignored inhomogeneous terms since they can be erased by using special solutions. We assume that m_Φ^2 and ω_X are almost constant in the timescale of $1/H$.

We estimate the effect of resonant particle production in quantum field theory by comparing $\varphi_{\mathbf{k}}$ and $\chi_{\mathbf{k}}$ with “free” solutions, $\varphi_{\mathbf{k}}^{\text{free}}$ and $\chi_{\mathbf{k}}^{\text{free}}$, which satisfy the same differential equations but without δm_φ^2 , δm_χ^2 or δm_{mix}^2 . Notice that $\chi_{\mathbf{k}}^{\text{free}}$ and $\varphi_{\mathbf{k}}^{\text{free}}$ should give the zero point fluctuations with appropriate normalization. Since $|\mathbf{k}|^2/a^2$ dominates over all the mass terms when $t \rightarrow -\infty$, we set

$$\lim_{t \rightarrow -\infty} \frac{\chi_{\mathbf{k}}}{\chi_{\mathbf{k}}^{\text{free}}} = \lim_{t \rightarrow -\infty} \frac{\varphi_{\mathbf{k}}}{\varphi_{\mathbf{k}}^{\text{free}}} = 1 . \quad (46)$$

To suppress the resonant particle production, we require⁷

$$N_\chi \left(\frac{|\mathbf{k}|^2}{a^2} \right) \lesssim \mathcal{O}(1) , \quad N_\varphi \left(\frac{|\mathbf{k}|^2}{a^2} \right) \lesssim \mathcal{O}(1) , \quad (47)$$

for all $|\mathbf{k}| > 3H/2$. Here,

$$N_\chi \left(\frac{|\mathbf{k}|^2}{a^2} \right) \equiv \frac{1}{2} \left| \frac{\chi_{\mathbf{k}}}{\chi_{\mathbf{k}}^{\text{free}}} \right|^2 - \frac{1}{2} , \quad N_\varphi \left(\frac{|\mathbf{k}|^2}{a^2} \right) \equiv \frac{1}{2} \left| \frac{\varphi_{\mathbf{k}}}{\varphi_{\mathbf{k}}^{\text{free}}} \right|^2 - \frac{1}{2} , \quad (48)$$

which we call the *occupation numbers*.

⁶ The sign of δm_{mix}^2 depends on that of α , but it is not important.

⁷ We do not consider the modes with $|\mathbf{k}| < 3H/2$ since they are super-horizon modes.

In the WKB approximation, $\chi_{\mathbf{k}}^{\text{free}}$ and $\varphi_{\mathbf{k}}^{\text{free}}$ are calculated as

$$\chi_{\mathbf{k}}^{\text{free}} \simeq \frac{C_{\chi}}{\left(m_{\chi}^2 + \frac{|\mathbf{k}|^2}{a^2(t)} - \frac{9}{4}H^2\right)^{1/4}} e^{i \int^t \sqrt{m_{\chi}^2 + \frac{|\mathbf{k}|^2}{a^2(t')} - \frac{9}{4}H^2} dt' - \frac{3}{2}Ht}, \quad (49)$$

$$\varphi_{\mathbf{k}}^{\text{free}} \simeq \frac{C_{\varphi}}{\left(m_{\varphi}^2 + \frac{|\mathbf{k}|^2}{a^2(t)} - \frac{9}{4}H^2\right)^{1/4}} e^{i \int^t \sqrt{m_{\varphi}^2 + \frac{|\mathbf{k}|^2}{a^2(t')} - \frac{9}{4}H^2} dt' - \frac{3}{2}Ht}, \quad (50)$$

where C_{χ} and C_{φ} are constants.

On the other hand, $\chi_{\mathbf{k}}$ and $\varphi_{\mathbf{k}}$ are well approximated by

$$\chi_{\mathbf{k}} \simeq \frac{C_{\chi}}{\sqrt{\mu_{\chi}(t)}} F_{\chi}(t) e^{i \int^t \mu_{\chi}(t') dt' - \frac{3}{2}Ht}, \quad (51)$$

$$\varphi_{\mathbf{k}} \simeq \frac{C_{\varphi}}{\sqrt{\mu_{\varphi}(t)}} F_{\varphi}(t) e^{i \int^t \mu_{\varphi}(t') dt' - \frac{3}{2}Ht}, \quad (52)$$

where μ_{χ} and μ_{φ} are the characteristic exponents, which will be given explicitly later. Here, F_{χ} and F_{φ} are $\mathcal{O}(1)$ functions satisfying

$$\lim_{t \rightarrow -\infty} F_{\chi}(t) = \lim_{t \rightarrow -\infty} F_{\varphi}(t) = 1. \quad (53)$$

One can easily check these are in good agreement with numerical solutions.

At the first approximation, the occupation numbers are given by

$$N_{\chi} \left(\frac{|\mathbf{k}|^2}{a^2} \right) \simeq \frac{1}{2} \exp \left[\int_{|\mathbf{k}|^2/a^2(t)}^{\infty} \frac{|\text{Im}(\mu_{\chi})|}{H} \frac{dK}{K} \right] - \frac{1}{2}, \quad (54)$$

$$N_{\varphi} \left(\frac{|\mathbf{k}|^2}{a^2} \right) \simeq \frac{1}{2} \exp \left[\int_{|\mathbf{k}|^2/a^2(t)}^{\infty} \frac{|\text{Im}(\mu_{\varphi})|}{H} \frac{dK}{K} \right] - \frac{1}{2}, \quad (55)$$

where

$$K(t') = \frac{|\mathbf{k}|^2}{a^2(t')}. \quad (56)$$

Since the smallest $|\mathbf{k}|/a$ gives the strongest constraints, we check

$$N_{\chi}^{\text{max}} \equiv N_{\chi} \left(\frac{9H^2}{4a^2} \right) \lesssim \mathcal{O}(1), \quad N_{\varphi}^{\text{max}} \equiv N_{\varphi} \left(\frac{9H^2}{4a^2} \right) \lesssim \mathcal{O}(1). \quad (57)$$

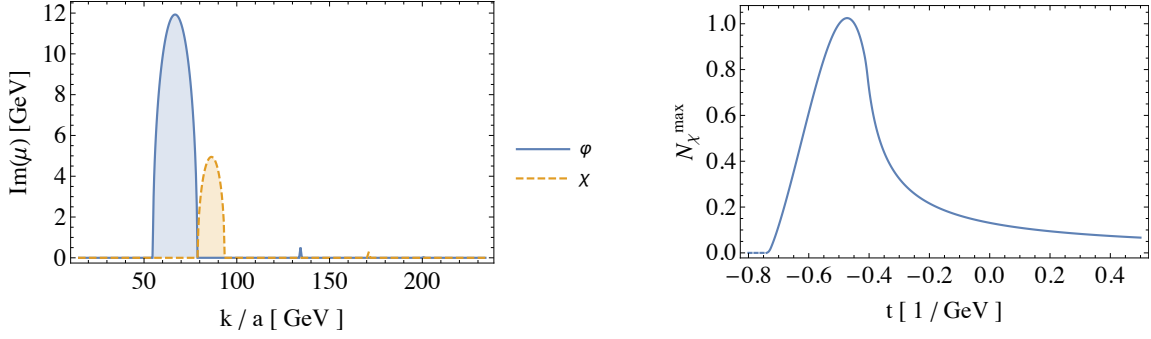


FIG. 4. *Left:* The characteristic exponents evaluated at $t = 0.3$. *Right:* the maximum occupation number of χ for each t .

A. Before the Higgs oscillation

Before the Higgs oscillation, Eqs. (39) and (40) are independent of each other and have the form of the Mathieu equation. In Appendix A, we obtain the characteristic exponents for the first and the second resonance bands, which are the strongest and the second strongest resonance bands, respectively.

In the left panel of Fig. 4, we plot the imaginary part of the characteristic exponents evaluated at $t = 0.3$, when the Higgs oscillation has not started yet. We evaluate them by directly solving the recurrence formula for $\Delta(0)$ in Appendix A. The largest peaks of μ_φ corresponds to the first resonance band and that of μ_χ corresponds to the second resonance band. We can see that there are tiny peaks in the right of the largest peaks. They correspond to the second resonance band of μ_φ and the third resonance band of μ_χ . Notice that the first resonance band for N_χ is what we use for the Higgs coherent oscillation, and hence it can not contribute to the particle production.

For the maximum occupation number of φ , we obtain $N_\varphi^{\text{max}} \simeq 0.5$. As for that of χ , we show its time dependence in the right panel of Fig. 4. For $t \lesssim -0.7$, the resonance condition can not be satisfied due to a large Higgs mass. It has a peak structure and we get $N_\chi^{\text{max}} \lesssim 1.0$. Since they are small enough, we can safely ignore the effect of particle production with this parameter set.

In the subsequent sections, we use the approximations given in Appendix A. They are

given by

$$|\text{Im}(\mu_\varphi(t))| \simeq \frac{\omega_X}{4} \text{Re} \left[\sqrt{\frac{\Lambda_0^8}{f^4 \omega_X^4} \left(1 - \frac{3}{32} \frac{\Lambda_0^8}{f^4 \omega_X^4} \right) - \left(\frac{4}{\omega_X^2} \left(\frac{|\mathbf{k}|^2}{a^2(t)} - \frac{9}{4} H^2 \right) - 1 + \frac{3}{8} \frac{\Lambda_0^8}{f^4 \omega_X^4} \right)^2} \right], \quad (58)$$

for the first resonance band of N_φ , and

$$|\text{Im}(\mu_\chi(t))| \simeq \frac{\omega_X}{8} \text{Re} \left[\sqrt{\frac{\Lambda_h^8}{\omega_X^8} - \left(\frac{4}{\omega_X^2} \left(m_\Phi^2 - \frac{9}{4} H^2 + \frac{|\mathbf{k}|^2}{a^2(t)} \right) - 4 - \frac{2}{3} \frac{\Lambda_h^4}{\omega_X^4} \right)^2} \right], \quad (59)$$

for the second resonance band of N_χ . Notice that the integration in Eqs. (54) and (55) can be executed analytically.

B. After the Higgs oscillation

After the Higgs oscillation begins, δm_{mix}^2 is turned on and $\varphi_{\mathbf{k}}$ and $\chi_{\mathbf{k}}$ are influenced by each other. In addition, the Higgs oscillation can cause resonant production of the W boson and the Z boson.

By solving Eqs. (39) and (40) directly, one finds that these differential equations have broad and strong instabilities. To avoid such instabilities, we restrict the number of the Higgs oscillations during the amplification to be $\mathcal{O}(1)$. Then, \mathcal{A}_h , m_Φ^2 and ω_X are different for each oscillation and we can avoid the exponential amplification of mode functions.

Another concern is that a single oscillation could produce too many particles, which might disturb the Higgs oscillation. Let us consider a generic particle, ζ , which has a mass of

$$m_\zeta^2 = g^2 \mathcal{A}_h^2 \cos^2 \left(\frac{\omega_X}{2} t \right), \quad (60)$$

where g is a coupling constant. In the following, we estimate how much ζ is produced for each oscillation. The adiabaticity condition is violated for momenta satisfying [46]

$$\frac{|\mathbf{k}|^2}{a^2} \lesssim \frac{1}{2\pi} g \mathcal{A}_h \omega_X, \quad (61)$$

whose occupation number becomes around one for a single oscillation. The energy density

of the created ζ particles is evaluated as

$$\varepsilon_\zeta \simeq \frac{1}{8\pi^2} \left(\frac{g\mathcal{A}_h\omega_X}{2\pi} \right)^2 . \quad (62)$$

Since it is much less than that of the Higgs oscillation,

$$\varepsilon_h \simeq \frac{\omega_X^2 \mathcal{A}_h^2}{4} , \quad (63)$$

we can safely neglect the effect of particle production.

As we can see from Fig. 3, the $\mathcal{O}(1)$ number of oscillations is indeed realized with the parameter set given in (34).

VI. VACUUM DECAY RATE

In this section, we review a vacuum decay rate, which will be used to evaluate the stability of a vacuum after the relaxation. As pointed out in the introduction, the lifetime of the first selected vacuum should be much longer than the age of the universe, otherwise one needs an unacceptably large number of e -folds to find a sufficiently long-lived vacuum.

We approximate the potential around the EW vacuum by a one-dimensional potential along X , which is given by

$$V \simeq -r\epsilon M^2 X - \frac{\Lambda_0^4 + \Lambda_h^2 v^2}{2} \cos \frac{X}{f} , \quad (64)$$

where $v \simeq 246$ GeV is the Higgs VEV.

The origin of X is redefined so that the correct EW vacuum corresponds to $X \simeq 0$, which we label as X_F . In the following, we evaluate the tunneling rate into the deeper vacuum around $X \simeq 2\pi f$, which we label as X_T . The decay rate is given by the bubble nucleation rate [47, 48], which is expressed as

$$\gamma = A e^{-B} . \quad (65)$$

Here,

$$B = S_E[X_B] - S_E[X_F] , \quad (66)$$

and X_B is the bounce solution. The prefactor A is assumed to be $(100 \text{ GeV})^4$ in our analysis⁸. For the evaluation of B , we use the thin wall approximation [47], which is given by

$$B_{\text{thin}} \equiv \frac{27\pi^2}{2} \frac{\sigma^4}{(V[X_F] - V[X_T])^3} , \quad (67)$$

where

$$\sigma = \int_{X_*}^{X_F} dX \sqrt{2(V[X] - V[X_F])} . \quad (68)$$

Here, X_* is a constant determined by

$$V[X_*] = V[X_F], \quad X_* \in [X_F, X_T] . \quad (69)$$

Since it gives a lower bound on B , we get an upper bound on the bubble nucleation rate as

$$\gamma_{\text{ub}} \equiv (100 \text{ GeV})^4 e^{-B_{\text{thin}}} . \quad (70)$$

The actual constraint of vacuum stability will be discussed in the following section together with other constraints.

VII. VIABLE PARAMETER SPACE FOR THE RELAXION MECHANISM

In this section, we summarize constraints on the parameters. We divide them into four categories; (i) those for the successful relaxation, (ii) those from consistency of our analysis, (iii) those from the explicit model of the strong sector, and (iv) those from experiments. The constraints of (i) are essential and independent of what are behind the relaxion potential, while those of (iii) depend on the detail of the strong sector. Some of the constraints of (ii) may be removed, but it is beyond the scope of this paper.

A. Successful Relaxation

1. Roll down

We first discuss the conditions for the relaxion to roll down the potential.

⁸ Since all the parameters are around the EW scale, we expect A is not so far from the EW scale.

The terminal velocity of the relaxion should be large enough so that the relaxion can go over the bumps, which gives

$$\frac{r\epsilon M^2}{3H} \gtrsim \Lambda_0^2, \text{ (Go over bumps).} \quad (71)$$

To violate the slow-roll condition, we require

$$\frac{3H\Lambda_0^4}{2fr\epsilon M^2} \gtrsim H, \text{ (Fast roll).} \quad (72)$$

The classical rolling should dominate over quantum fluctuations, which gives

$$\frac{H}{2\pi} \lesssim \frac{r\epsilon M^2}{3H^2}, \text{ (Classical roll).} \quad (73)$$

2. Stopping mechanism

Next, we discuss the conditions to stop the relaxion at the desired position.

The existence condition of the edge solution can be read off from Eqs. (30) and (32) with $\mathcal{A}_h = 0$. It is given by

$$\frac{r\epsilon M^2}{\Lambda_h^2 f} \lesssim 1, \text{ (Edge solution).} \quad (74)$$

The Higgs oscillation should start before the relaxion scans the correct Higgs mass. It gives

$$m_\Phi^2(t_{\text{start}}) > m_\Phi^2(t_{\text{end}}), \text{ (Do not pass through),} \quad (75)$$

where

$$m_\Phi^2(t_{\text{start}}) \simeq \frac{r^2\epsilon^2 M^4}{36f^2 H^2} + \frac{\Lambda_h^2}{2} - \frac{r^2\epsilon^2 M^4}{4f^2 \Lambda_h^2} - \frac{9H^2(2\Lambda_0^4 \Lambda_h^2 + f^2 \Lambda_h^4)}{8r^2\epsilon^2 M^4}, \quad (76)$$

$$m_\Phi^2(t_{\text{end}}) \simeq -\frac{\lambda}{4}v^2 + \Lambda_h^2 \sqrt{1 - \left(\frac{2fr\epsilon M^2}{\Lambda_0^4 + \Lambda_h^2 v^2} \right)^2}. \quad (77)$$

When the relaxion hits a bump, the Higgs boson should acquire a large enough VEV to anchor the relaxion. We require the amplitude of the Higgs oscillation be smaller than the EW vacuum, namely,

$$\mathcal{A}_h(t_{\text{end}}) < v, \text{ (Anchor).} \quad (78)$$

3. *EW vacua*

Lastly, we discuss the conditions related to the EW vacuum.

There must be a stationary point of the relaxion potential around the EW vacuum, which gives

$$\frac{2fr\epsilon M^2}{\Lambda_0^4 + \Lambda_h^2 v^2} < 1 \text{ , (Stationary point) .} \quad (79)$$

To avoid fine-tuning, there should be a sufficient number of vacua that realize the Higgs mass around the EW scale, which gives

$$2\pi\epsilon f \lesssim v^2 \text{ , (Many vacua) .} \quad (80)$$

To make the lifetime of the EW vacuum longer than the age of the Universe, we require

$$\gamma_{\text{ub}} \lesssim H_0^4 \text{ , (Vacuum stability) ,} \quad (81)$$

with H_0 being the current value of the Hubble constant. It is equivalent to $B_{\text{thin}} \gtrsim 400$.

B. Consistency of Analysis

Since we assume that the inflaton potential dominates the total energy density during the relaxation, we require

$$H \gtrsim \sqrt{\frac{rM^4}{3M_{\text{Pl}}^2}} \text{ ,} \quad (82)$$

with M_{Pl} being the reduced Planck mass.

For the approximation used in Eq. (76) to be reliable, we need

$$\frac{r^2\epsilon^2 M^4}{36f^2 H^2} \gtrsim \left| \frac{\Lambda_h^2}{2} - \frac{r^2\epsilon^2 M^4}{4f^2 \Lambda_h^2} - \frac{9H^2(2\Lambda_0^4 \Lambda_h^2 + f^2 \Lambda_h^4)}{8r^2\epsilon^2 M^4} \right| . \quad (83)$$

To avoid the resonant particle production before the Higgs oscillation starts, we require

$$N_{\chi}^{\text{max}} \lesssim \mathcal{O}(1) \text{ , } N_{\varphi}^{\text{max}} \lesssim \mathcal{O}(1) . \quad (84)$$

To avoid the resonant particle production after the Higgs oscillation starts, we require

$$N_{\text{osc}} \equiv \frac{1}{2} \frac{m_{\Phi}^2(t_{\text{start}}) - m_{\Phi}^2(t_{\text{end}})}{2\pi\epsilon f} \lesssim \mathcal{O}(10) . \quad (85)$$

Notice that not all of them are responsible for the particle production since the amplitude is small for the first several oscillations.

C. Model of Strong Sector

The parameters coming from the new strong sector, Λ_0 and Λ_h , should be obtained naturally from an explicit model. In our analysis, we adopt the simplest model described in Section II.

Since we need fermions that condensate, we require

$$m_N^{(\text{eff})} \lesssim \Lambda_c . \quad (86)$$

To restrict effects of the new doublet fermions on the strong dynamics, we require

$$\Lambda_c \lesssim m_L . \quad (87)$$

The Hubble expansion should not disturb the condensation, which gives

$$H \lesssim \Lambda_c . \quad (88)$$

To keep the new Yukawa couplings perturbative, we require

$$\max(|y|, |\tilde{y}|) \lesssim 4\pi . \quad (89)$$

Since there are tree and quantum contributions in Λ_0^4 , there can be an implicit cancellation. To avoid a fine-tuning, we define fine-tuning parameter ξ as

$$\xi = \frac{\frac{y\tilde{y}}{8\pi^2} m_L \ln \frac{M^2}{m_L^2} - m_N}{\frac{y\tilde{y}}{8\pi^2} m_L \ln \frac{M^2}{m_L^2}} , \quad (90)$$

and require

$$|\xi| \gtrsim 0.1 . \quad (91)$$

Notice that, once m_L and Λ_c are fixed, the other parameters are determined as

$$y\tilde{y} = -\frac{\Lambda_h^2 m_L}{\Lambda_c^3} , \quad (92)$$

$$m_N^{(\text{eff})} = \frac{\Lambda_0^4 + \Lambda_h^2 v^2}{2\Lambda_c^3} , \quad (93)$$

$$\xi = \frac{4\pi^2 \Lambda_0^4}{m_L^2 \Lambda_h^2 \ln \frac{M^2}{m_L^2}} . \quad (94)$$

D. Experiments

1. Strong sector

We first discuss experimental constraints on the new strong sector.

From Eq. (94), we expect that m_L is not much larger than Λ_0 to avoid a fine-tuning. The constraints on the new doublet fermions have been discussed in [42] in the context of the original relaxion mechanism. They evaluate the contributions to the six EW precision valuables, (S, T, U, V, W, X) , and show the 95% confidence level (CL) excluded region on the $(m_L, y = \tilde{y})$ plane. For example, for $m_L \gtrsim 200$ GeV, we can take $|y\tilde{y}| \lesssim 0.1$, and for $m_L \gtrsim 500$ GeV, we can take $|y\tilde{y}| \lesssim 0.4$. They also discuss the constraints from collider searches, which can be avoided if $m_L \gtrsim 200$ GeV.

Next, we discuss the constraints on the mesons in the new strong sector. In our mechanism, all the new mesons naturally have masses around or larger than the Higgs mass. This is because the Higgs mass is determined mainly by Λ_h , and Λ_c is typically larger than Λ_h , as can be seen from Eq. (9). Since the anomalous axial symmetry is the only broken symmetry, all the states in the strong sector are expected to have masses around or larger than Λ_c .

If new mesons have mass around the EW scale, some of them can mix with the Higgs boson and decrease the signal strengths of the Higgs boson. For simplicity, we avoid such mixing by taking

$$\Lambda_c \gtrsim 400 \text{ GeV} . \quad (95)$$

Then, they effectively decouple from Higgs phenomenology.

Lastly, we comment on the dynamics that gives the relaxion decay constant, f . As we will discuss in Section IX, we consider that it comes from condensation of new fermions in order to avoid fine-tuning. Then, we expect a rich spectrum around $4\pi f$. Since we consider $f \simeq 100$ GeV, the particles are around 1 TeV and thus we can safely ignore their effects.

2. Relaxion and Higgs boson

Let us move on to the collider constraints on the relaxion and the Higgs boson.

Since we assume a rather small f , the relaxion easily mixes with the Higgs boson. We define the mixing angles as

$$s_X \equiv -\sin \frac{\langle X \rangle}{f} = \frac{2fr\epsilon M^2}{\Lambda_0^4 + \Lambda_h^2 v^2}, \quad c_X \equiv -\cos \frac{\langle X \rangle}{f} = \sqrt{1 - s_X^2}, \quad (96)$$

where $\langle X \rangle$ is the expectation value of the relaxion at the EW vacuum.⁹ Using these, the mass matrix of the scalars are expressed as

$$\begin{pmatrix} \frac{\lambda v^2}{2} & \frac{\Lambda_h^2 v}{f} s_X \\ \frac{\Lambda_h^2 v}{f} s_X & \frac{\Lambda_0^4 + \Lambda_h^2 v^2}{2f^2} c_X \end{pmatrix}, \quad (97)$$

in the basis of (χ, φ) .¹⁰

When θ is small, the mixing angle of χ and φ can be calculated as

$$\theta \simeq \frac{-2fv\Lambda_h^2 s_X}{(\Lambda_0^4 + v^2\Lambda_h^2)c_X - \lambda f^2 v^2}. \quad (98)$$

Here, the mixing angle is defined by

$$\begin{pmatrix} h_{125} \\ S \end{pmatrix} = \begin{pmatrix} c_\theta & -s_\theta \\ s_\theta & c_\theta \end{pmatrix} \begin{pmatrix} \chi \\ \varphi \end{pmatrix}, \quad (99)$$

where h_{125} is the 125GeV Higgs boson and S is the relaxion-like boson. The masses of h_{125}

⁹ In the absence of ϵ , the relaxion settles at $\sin\langle X \rangle/f = 0$ and $\cos\langle X \rangle/f = -1$.

¹⁰ The coupling between the relaxion and the Higgs boson, $\epsilon X|\Phi|^2$, does not affect the collider phenomenology since ϵ is small.

and S are approximately given by

$$m_{125}^2 = \frac{\lambda v^2}{2} + 2\theta \frac{\Lambda_h^2 v}{f} s_X , \quad (100)$$

$$m_S^2 = \frac{\Lambda_0^4 + \Lambda_h^2 v^2}{2f^2} c_X - 2\theta \frac{\Lambda_h^2 v}{f} s_X , \quad (101)$$

respectively. Since the Higgs mass has been measured, we tune λ so that it reproduces

$$m_{125} = 125 \text{ GeV} . \quad (102)$$

Here, we ignore the uncertainty since it has very little effect on our results.

Since S has couplings to the SM particles through the mixing, it can be produced at colliders. We assume that S decays only into the SM particles. The partial decay widths of the relaxion are given by

$$\Gamma(S \rightarrow 2h_{125}) \simeq \frac{1}{32\pi} \frac{|g_{Shh}|^2}{m_S} \sqrt{1 - \frac{4m_{125}^2}{m_S^2}} , \quad (103)$$

$$\Gamma(S \rightarrow \text{SM}) = s_\theta^2 \times \Gamma(h_{125} \rightarrow \text{SM})|_{m_{125} \rightarrow m_S} , \quad (104)$$

where

$$g_{Shh} = \frac{3\lambda v}{2} c_\theta^2 s_\theta - \frac{2v\Lambda_h^2}{f^2} (2c_\theta^2 s_\theta - s_\theta^3) c_X - \frac{\Lambda_h^2}{f} (2c_\theta s_\theta^2 - c_\theta^3) s_X - \frac{\Lambda_0^4 + \Lambda_h^2 v^2}{2f^3} c_\theta s_\theta^2 s_X , \quad (105)$$

and $\Gamma(h_{125} \rightarrow \text{SM})|_{m_{125} \rightarrow m_S}$ is the Higgs partial decay width with the Higgs mass being replaced by m_S .¹¹

The experiments at LEP, Tevatron, and LHC have extensively searched for neutral Higgs bosons. In our analysis, we use `HiggsBounds`[49–53] to obtain the 95% CL excluded region.

Finally, we discuss the Higgs phenomenology. To avoid the constraints on the Higgs signal strengths, we require [42, 54]

$$c_\theta^2 \gtrsim 0.8 , \quad (106)$$

as a reference¹². In particular, the branching ratio of the Higgs boson into two relaxions

¹¹ We neglect possible decay of the relaxion into two photons through the strong sector.

¹² By using the P-value of `HiggsSignals` [54, 55], the number is about 0.7 at 95% CL. The ATLAS and the CMS collaborations provide global fits of the signal strengths, which give about 0.95 at 95%CL since the central values are rather high [56, 57].

easily dominates over the others due to a large coupling,

$$g_{hSS} \simeq \frac{v\Lambda_h^2}{f^2} c_X . \quad (107)$$

Thus, we forbid it kinematically by requiring

$$\frac{m_{125}}{2} < m_S . \quad (108)$$

Notice that all the collider constraints can be avoided if the relaxion mass and the Higgs mass are degenerated. However, we do not consider such a region to avoid additional fine-tuning.

VIII. PARAMETER REGION

In this section, we present an example parameter region. To reduce the number of parameters, we fix the following parameters in this section;

$$H = 10 \text{ GeV} , \epsilon = 0.8 \text{ GeV} , r = 0.002 , M = 20 \text{ TeV} . \quad (109)$$

In addition, we restrict $\Lambda_0 = \Lambda_h$. If not explicitly specified, λ is chosen so that it reproduces the observed Higgs mass.

The conditions for the successful relaxation are shown in Fig. 5. We show only those of Eqs. (71), (72), (74), and (75), which give the strongest bounds with the parameter set given in (109). The shaded regions are excluded by the reasons described in the legend. As we can see, the allowed region is not small, so that we do not need to fine-tune the parameters.

Let us move on to the constraints from the consistency of our analysis. In Fig. 6, we show where our analysis becomes unreliable. The blue region is the same as in Fig. 5 but all the constraints are combined. In the left panel, the orange shaded region violates Eq. (83), where we can not use the analytic relations for the edge solution. The red lines in the same panel show the number of Higgs oscillations. To avoid the resonant particle production, this should not be so large. Since this is a very rough approximation, we assume

$$N_{\text{osc}} \lesssim 25 , \quad (110)$$

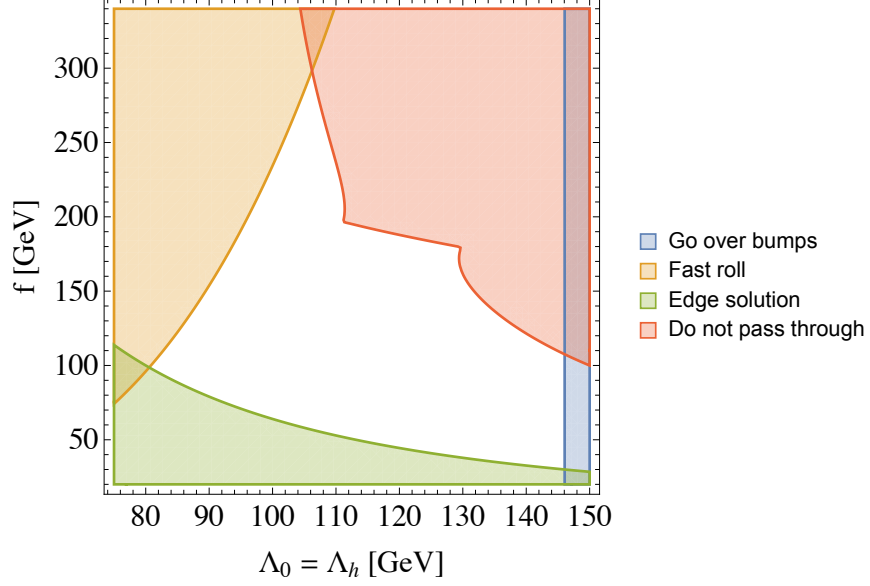


FIG. 5. The conditions for the successful relaxation. We plot only the strongest ones. The blue shaded region around the right edge is excluded by “Go over bumps” condition. The orange shaded region around the upper left corner is excluded by “Fast roll” condition. The green shaded region around the bottom left corner is excluded by “Edge solution” condition. The red shaded region around the upper right corner is excluded by “Do not pass through” condition.

is safe.

The right panel shows of Fig. 6 shows the maximum occupation numbers of φ and χ before the Higgs oscillation starts. These numbers should be small enough so that the assumption of homogeneous fields is a good approximation. In this analysis, we assume

$$N_{\varphi}^{\max} \lesssim 10, \quad N_{\chi}^{\max} \lesssim 10, \quad (111)$$

are safe.

Next, we discuss the constraints on the strong sector. To illustrate them, let us take

$$\Lambda_c = 400 \text{ GeV}, \quad \lambda = 0.52. \quad (112)$$

In Fig. 7, we plot $|y\tilde{y}|$, ξ , and $m_N^{(\text{eff})}$. Since the first two depend on m_L , we show also the m_L dependencies in the left panel. As we can see, the fine-tuning parameter, ξ , is $\mathcal{O}(0.1)$, and thus the parameter is not so tuned. In addition, $|y\tilde{y}|$ and M_N are small enough, so that the conditions of Eqs. (86) and (89) are satisfied. Since the doublet fermions are heavier than

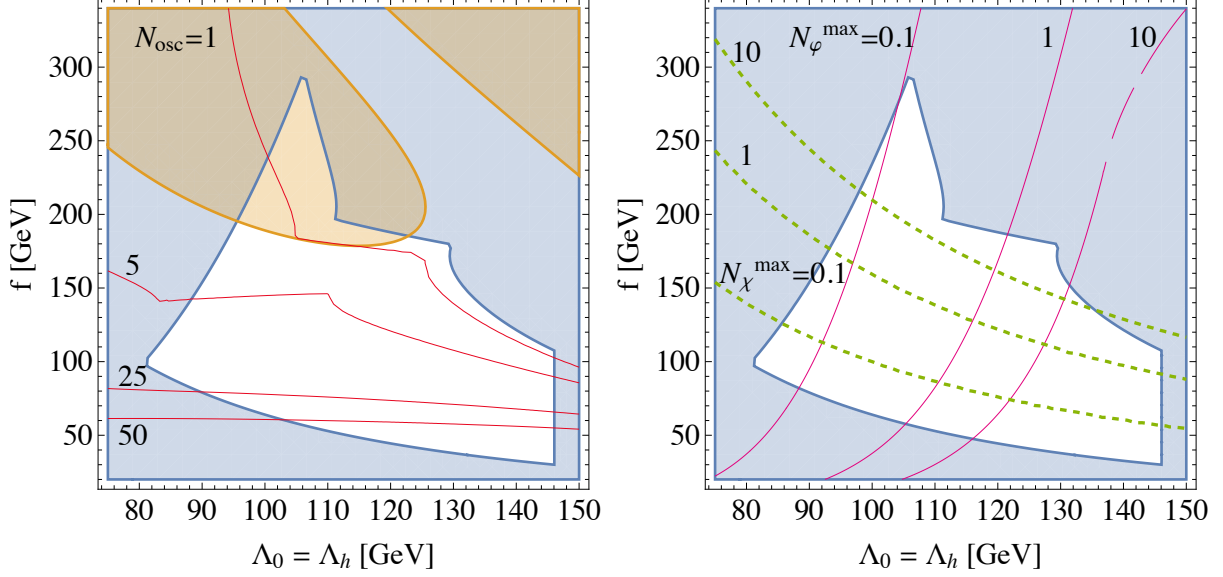


FIG. 6. Consistency check of our analysis. The blue shaded region is a summary of Fig. 5. *Left:* The orange shaded region violates Eq. (83). The red lines show the estimate of the number of Higgs oscillation, $N_{\text{osc}} = 1, 5, 25, 50$. *Right:* The maximum occupation number produced before the Higgs oscillation. The red solid lines correspond to $N_{\phi}^{\text{max}} = 0.1, 1, 10$ and the green dashed ones correspond to $N_{\chi}^{\text{max}} = 0.1, 1, 10$.

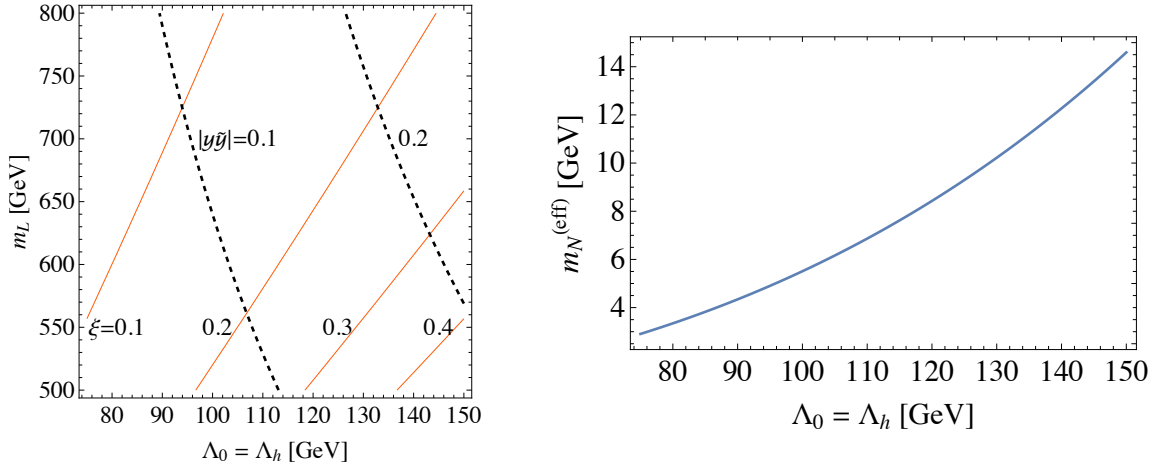


FIG. 7. The parameters in the model of strong sector. *Left:* The black dashed lines indicate $|y\tilde{y}| = 0.1, 0.2$ and the red solid lines indicate $\xi = 0.1, 0.2, 0.3, 0.4$. *Right:* The lightest fermion mass in the strong sector.

500 GeV, we can avoid the constraints from the EW precision and the resonance searches.

Finally, we show the collider constraints on the relaxion and the Higgs signal strengths. In Fig. 8, we shade the excluded region with green, which comes mainly from the searches for the relaxion. The blue region is the same as in Fig. 7 and the orange region violates the

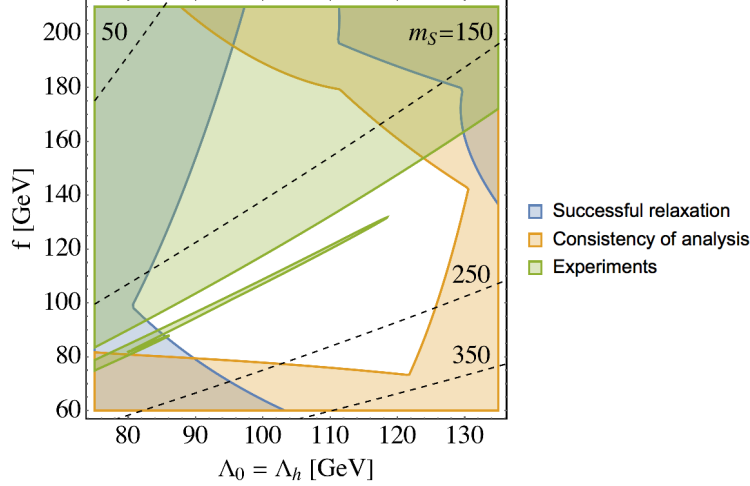


FIG. 8. The experimental constraints. The blue and the orange shaded regions are summaries of Figs. 5 and 6, respectively. The green region is excluded either by the collider searches at the 95% CL, or by the Higgs signal strength measurements. The black dashed lines indicates $m_S = 50, 150, 250, 350$.

consistency conditions, namely, Eqs. (83), (110) and (111). We plot m_S with black dashed lines. In the allowed region, the main decay modes of the relaxion are typically WW and ZZ . Around the bottom right corner of the allowed region, we have a region with $m_S > 2m_{125}$, where the $S \rightarrow hh$ channel opens. It tends to dominate the decay width. The narrow green band comes from the low-mass end of the LHC constraints.

We pick up some sample points within the allowed region, which are shown with stars in the left panel of Fig. 9. In the right panel, we plot the evolution of the Higgs homogeneous mode for each sample point. The Higgs oscillations are expected to start at $t = 1 \text{ GeV}^{-1}$. As we can see, the relaxation is successful for these sample points. We summarize phenomenology for each example point in Table I.

At Point 3, the Higgs oscillation does not start. It is simply because the parameter set is around the boundary of Eq. (74). Even so, the relaxation is successful and it corresponds to the other mechanism explained in Appendix C.

IX. THE RELAXION POTENTIAL AND COSMOLOGICAL HISTORY

In the preceding sections, we have discussed the dynamics of the relaxion and the Higgs field assuming that their potential is given by Eq. (4). The most important feature of the

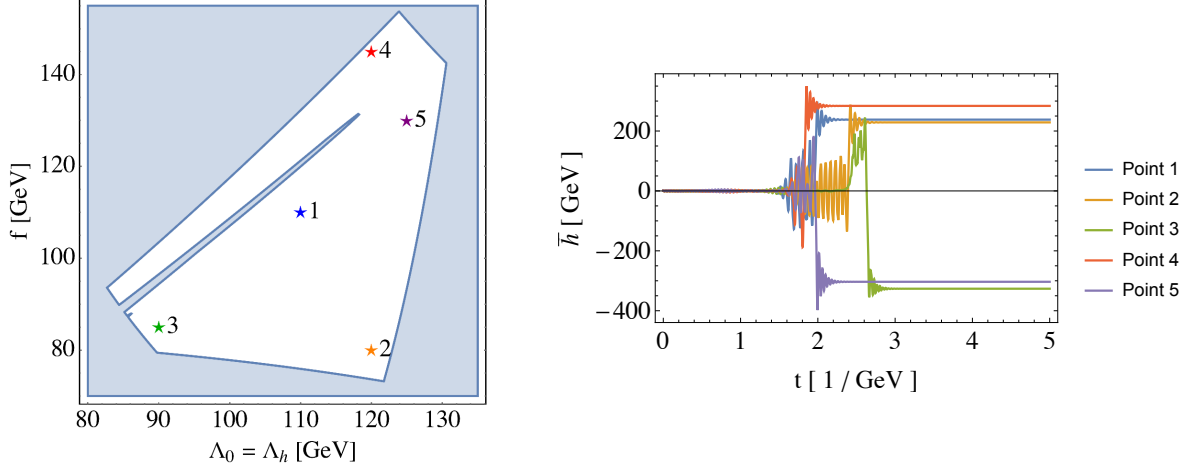


FIG. 9. The evolution of the Higgs field for each sample point. The locations of sample points are shown in the left panel. For each point, the evolution of the Higgs field is shown in the right panel.

Point	$\Lambda_0 = \Lambda_h$ [GeV]	f [GeV]	B_{thin}	N_{φ}^{max}	N_{χ}^{max}	m_S [GeV]	s_{θ}	$\text{BR}(S \rightarrow 2h_{125})$
1	110	110	39715	0.63	0.29	192	-0.22	0
2	120	80	73916	5.18	0.12	290	-0.06	0.79
3	90	85	9186	0.11	0.03	197	-0.21	0
4	120	145	71693	1.33	3.49	165	-0.41	0
5	125	130	101498	3.76	2.32	189	-0.22	0

TABLE I. Phenomenology at the example points

potential is the shift symmetry of X that is broken by two distinct sources. In this section, we demonstrate that such a potential can naturally arise if we identify the relaxion with a pseudo NGB. We also discuss cosmological history that is compatible with the fast-rolling relaxion.

A. Pseudo Nambu-Goldstone Relaxion

Since the pseudo NGB should reside in a compact field space, we expect that the relaxion potential has a form of

$$V(X) = \kappa_H (rM^2 + |\Phi|^2) F_H^2 \cos\left(\frac{X}{F_H}\right) + \Lambda^4 (|\Phi|^2) \cos\left(\frac{X}{F_L} + \delta\right). \quad (113)$$

Here, we introduced two energy scales, F_H and F_L , which are associated with spontaneous breaking of a global $U(1)$ symmetry. We take F_L to be f in Eq. (4), while F_H to be very large so that it reproduces the linear potential of the relaxion. The X -dependence of the

potential arises from explicit breaking of the global $U(1)$ symmetry. An arbitrary phase, δ , is irrelevant in the following discussion.

Before discussing an explicit model that generates Eq. (113), let us first clarify the relation between Eq. (113) and Eq. (4).

To identify the first term in Eq. (113) as the linear potential in Eq. (4), we need a large enough F_H . Since the relaxion needs to scan its field range of $\mathcal{O}(M^2/\epsilon)$ to find the EW scale, we require

$$F_H \gtrsim \frac{M^2}{\epsilon} . \quad (114)$$

The coefficient of the linear potential in Eq. (4) is obtained by expanding X around an arbitrary point, X_0 , as

$$X = X_0 + \delta X. \quad (115)$$

Then, we have¹³

$$\epsilon = \kappa F_H \sin\left(\frac{X_0}{F_H}\right) . \quad (116)$$

The first term in Eq. (113) also contributes to the Higgs mass squared by

$$\Delta M^2 = \epsilon F_H \cot\left(\frac{X_0}{F_H}\right) , \quad (117)$$

at $X \simeq X_0$. It should not exceed $\mathcal{O}(M^2)$ since we assume the natural scale of the Higgs mass squared is $\mathcal{O}(M^2)$. Together with the constraint of Eq. (114), F_H should satisfy

$$F_H \sim \frac{M^2}{\epsilon} . \quad (118)$$

For example, if we take $F_H \simeq 5 \times 10^8 \text{ GeV}$ and $\kappa_H \simeq 10^{-9}$, we have $\epsilon \simeq 0.8 \text{ GeV}$ and $M \simeq 20 \text{ TeV}$.¹⁴

In Fig. 10, we show an illustration of the relaxion potential with $F_H = 40F_L$. The larger structure of the potential is governed by the first term in Eq. (113), while the small wiggle comes from the second term. We close up the potential around $X_0/F_H = \pi/3$ for a small

¹³ We assume that X_0 is not accidentally very close to an extremum of $\cos(X/F_H)$.

¹⁴ A hierarchy between F_H and M can be stabilized, for example, by supersymmetry with M being the soft scalar mass of the Higgs doublets.

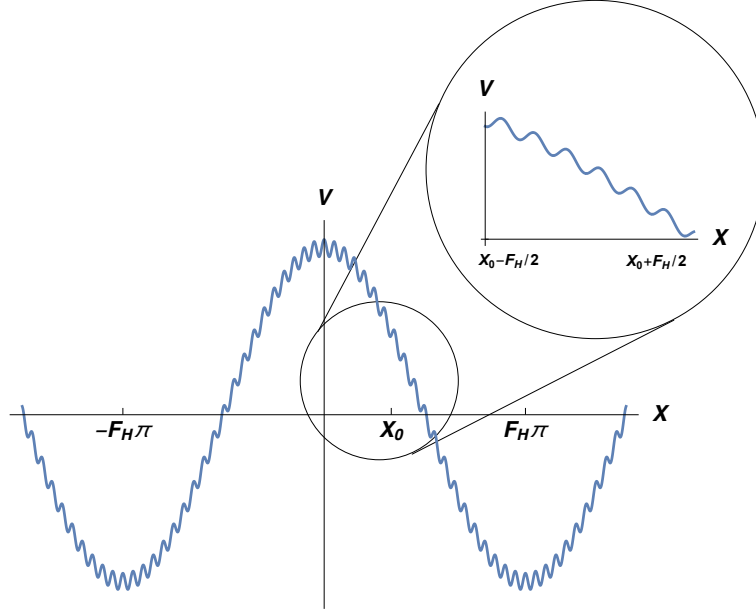


FIG. 10. An illustration of the relaxation potential of Eq. (113) with $F_H = 40F_L$. The small wiggle comes from the second term in Eq. (113). The inserted figure is a close-up of the potential around $X_0/F_H = \pi/3$.

interval, $\delta X \in [-F_H/2, F_H/2]$, to illustrate that it is well approximated by a linear potential with a small modulation.

B. Relaxion Potential from Clockwork Mechanism

Here, we discuss an explicit model that generates Eq. (113). As we have mentioned, the X -dependence of the potential originates from explicit breaking of the global symmetry. A difficulty in model building is that we need two hierarchical decay constants, F_H and F_L .

Let us first consider a global $U(1)$ symmetry that is broken by two condensation operators; one is at $\mathcal{O}(F_H)$ and the other is at $\mathcal{O}(F_L)$. We assume that the $U(1)$ charges of these operators are the same. We consider an effective scalar potential given by

$$V(X) = \frac{1}{2}\kappa_H (rM^2 + |\Phi|^2) F_H^2 e^{i\frac{\pi_H}{F_H}} + \frac{1}{2}\Lambda^4 (|\Phi|^2) e^{i\frac{\pi_L}{F_L}} - gF_H^2 F_L^2 e^{i(\frac{\pi_H}{F_H} - \frac{\pi_L}{F_L})} + h.c. , \quad (119)$$

where π_H and π_L are the phase components of the condensation operators. It has a similar structure to that of Eq. (113), but we also have the third term, which is consistent with the

$U(1)$ symmetry defined as

$$\frac{\pi_H}{F_H} \rightarrow \frac{\pi_H}{F_H} + \alpha, \quad \frac{\pi_L}{F_L} \rightarrow \frac{\pi_L}{F_L} + \alpha, \quad \alpha = [0, 2\pi). \quad (120)$$

We assume that coefficient g is order one and thus the third term has the largest coefficient. Since one of the linear combinations of π_H and π_L becomes very heavy because of the third term, we identify the other lighter combination as the relaxion.

The potential of Eq. (119), however, does not provide the desirable relaxion potential of Eq. (113). In the limit of vanishing explicit breaking, the mass eigenstates of π_H and π_L are given by

$$\begin{pmatrix} X_H \\ X \end{pmatrix} = \frac{F_H F_L}{\sqrt{F_H^2 + F_L^2}} \begin{pmatrix} F_H^{-1} & -F_L^{-1} \\ F_L^{-1} & F_H^{-1} \end{pmatrix} \begin{pmatrix} \pi_H \\ \pi_L \end{pmatrix}. \quad (121)$$

Thus, we find that π_H and π_L include X component as

$$\frac{\pi_H}{F_H} = \frac{X}{\sqrt{F_H^2 + F_L^2}} \simeq \frac{X}{F_H}, \quad \frac{\pi_L}{F_L} = \frac{X}{\sqrt{F_H^2 + F_L^2}} \simeq \frac{X}{F_H}, \quad (122)$$

and hence both of the first two terms in Eq. (119) give the same decay constant of the relaxion around F_H .¹⁵

This difficulty can be circumvented by introducing a hierarchical $U(1)$ charge between the two condensation operators. When the operator corresponding to π_H has charge $Q_H \ll 1$, the third term is modified as

$$V(X) = \frac{1}{2} \kappa_H (r M^2 + |\Phi|^2) F_H^2 e^{i \frac{\pi_H}{F_H}} + \frac{1}{2} \Lambda^4 (|\Phi|^2) e^{i \frac{\pi_L}{F_L}} - g F_H^2 F_L^2 e^{i \left(\frac{\pi_H}{F_H} - \frac{Q_H \pi_L}{F_L} \right)} + h.c. \quad (123)$$

Here, the $U(1)$ symmetry is realized by

$$\frac{\pi_H}{F_H} \rightarrow \frac{\pi_H}{F_H} + Q_H \alpha, \quad \frac{\pi_L}{F_L} \rightarrow \frac{\pi_L}{F_L} + \alpha, \quad \alpha = [0, 2\pi). \quad (124)$$

In this case, the relaxion component of π_H and π_L are given by

$$\frac{\pi_H}{F_H} = \frac{X}{\sqrt{F_H^2 + F_L^2 / Q_H^2}}, \quad \frac{\pi_L}{F_L} = \frac{X}{Q_H \sqrt{F_H^2 + F_L^2 / Q_H^2}}. \quad (125)$$

¹⁵ This is obvious from the fact that the NGB mostly resides in the phase component of the first condensation operator.

Thus, with $F_H \sim F_L/Q_H$, we achieve

$$\frac{\pi_H}{F_H} \sim \frac{X}{F_H}, \quad \frac{\pi_L}{F_L} \sim \frac{X}{F_L}. \quad (126)$$

Substituting Eq.(126) to the potential in Eq.(123), we obtain the desirable potential of Eq.(113) with $F_H \gg F_L$.

It should be noted that an exponentially small Q_H can be achieved by the clockwork mechanism [58–60] (see also [61]). For example, let us consider $N + 1$ sectors containing condensation operators. We assume the charges of these operators decrease in geometric progression with ratio q^{-1} ($q > 1$). Identifying the phase component of the operator in the first sector as π_L and that in the $(N + 1)$ -th sector as π_H , we effectively get an exponentially small charge of $Q_H = q^{-N}$. For example, the hierarchy between $F_H \simeq 5 \times 10^8 \text{ GeV}$ and $F_L \simeq 10^2 \text{ GeV}$ is realized with $q = 3$ and $N = 14$.¹⁶

Finally, let us comment on the origin of the explicit breaking terms. For simplicity, we set all the condensation scales of $N + 1$ sectors to be around F_L . Then, the second term in the potential in Eq.(123) can be obtained by using the model in Section II with $X/f \rightarrow \pi_L/F_L$.

Similarly, we can construct a model that gives the first term in the potential in Eq.(123). Let us consider a new strong sector that couples to π_H , whose Lagrangian is given by¹⁷

$$\mathcal{L} = -\frac{1}{32\pi^2} \frac{\pi_H}{F_H} G_{H\mu\nu}^a \tilde{G}_H^{a\mu\nu} + M_N N_H N_H^c + M_L L_H L_H^c + y_H \Phi L_H N_H^c + \tilde{y}_H \Phi^\dagger L_H^c N_H. \quad (127)$$

Here, G_H denotes the field strength of a new $SU(3)$ gauge group. The new fermions, N_H and L_H , are in the fundamental representation of $SU(3)$ and correspond to N and L in Section II, respectively. Assuming that L_H is heavier than the dynamical scale, Λ_H , and N_H is lighter, we find

$$rM^4 \sim \kappa_H r M^2 F_H^2 \sim M_N \Lambda_H^3, \quad (128)$$

$$M^2 \sim \kappa_H F_H^2 \sim \frac{\tilde{y}_H y_H}{M_L} \Lambda_H^3. \quad (129)$$

With these relations, we find, for example, that $M \simeq 30 \text{ TeV}$ and $\epsilon \simeq 0.1 \text{ GeV}$ can be achieved with $M_L \sim \Lambda_H \simeq M$, $\tilde{y}_H y_H = \mathcal{O}(1)$, and $M_N/M_L \sim (\tilde{y}_H) y_H r$.¹⁸

¹⁶ The smallness of F_L does not re-introduce a hierarchy problem if we adopt dynamical symmetry breaking in each sector [62].

¹⁷ In fact, the potential in Eq.(113) can be achieved without introducing condensation of $\mathcal{O}(F_H)$ since we could attach condensation of $\mathcal{O}(F_L)$ to the $(N + 1)$ -th sector. As we will see below, however, the condensation of $\mathcal{O}(F_H)$ offers simple cosmological history.

¹⁸ The mass squared, M_N , is required to be at least of $\mathcal{O}(\tilde{y}_H y_H / 16\pi^2 M_L)$ to be technically natural.

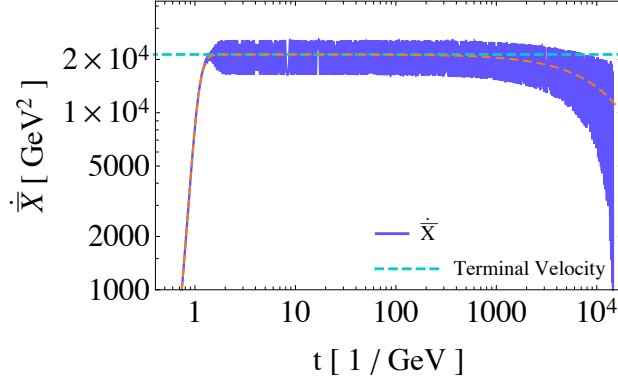


FIG. 11. The evolution of \dot{X} during inflation with $|\Phi| = 0$ (blue line). Low scale inflation with the Hubble constant $H = 10 \text{ GeV}$ is assumed to take place after radiation domination. (The time variable t can be regarded as an e -folding number, $\mathcal{N}_e = Ht$.) During radiation domination, the strong dynamics responsible for the relaxion potential in Eq. (113) does not exhibit confinement, and hence, the relaxion does not have any potential. The first dynamics confines at $T \simeq \Lambda_H$, which generates the first term in Eq. (113), and the relaxion is accelerated. The second dynamics confines at $T \simeq \Lambda_c$, which modulate the relaxion potential. The dashed cyan line shows the terminal velocity expected for a purely linear potential. The dashed orange line shows the evolution of \dot{X} without the second term in Eq. (113).

C. Cosmological History

In our mechanisms, we assume that the initial velocity of the relaxion is large enough so that it can go over the bumps created by the strong dynamics. In this section, we discuss cosmological history where the relaxion starts to roll before or during inflation.

A simple possibility is that there is a radiation dominated era before the relaxion mechanism takes place. We assume that the maximal temperature is high enough so that all the terms in Eq. (113) vanish. The succeeding inflation era starts typically before these terms are recreated. In the inflation era, the temperature decreases very quickly and the first dynamics confines at $T \simeq \Lambda_H$, which generates the first term in Eq. (113).¹⁹ It accelerates the relaxion unless the relaxion accidentally sits around an extremum. The relaxion reaches the terminal velocity within about one e -fold after the first confinement. Subsequently, the second dynamics confines at $T \simeq \Lambda$, which generates the second term in Eq. (113). If the relaxion has been accelerated enough, it can go over the created bumps, which explains the origin of the fast-rolling.

In Fig. 11, we show the time evolution of \dot{X} during inflation (blue line), ignoring the Higgs

¹⁹ Here, we assume that the global $U(1)$ symmetry has been broken well before the inflation starts.

field. Here, we assume that the inflation era starts at $t \sim \mathcal{O}(0.1) \text{ GeV}^{-1}$ with $H = 10 \text{ GeV}$. The parameters are taken to be $\epsilon = 0.8 \text{ GeV}$, $r = 0.002$, $M = 20 \text{ TeV}$, $F_H = 5 \times 10^8 \text{ GeV}$, $\Lambda_H = M$, and $F_L = \Lambda = 100 \text{ GeV}$. The initial condition of X is set to be $X = F_H(\pi - 1)$ and $\dot{X} = 0$ at $t = 0.05 \text{ GeV}$. In the analysis, we turn on the first and the second terms in Eq. (113) at $T \simeq \Lambda_H$ and $T \simeq \Lambda$, respectively. For comparison, we show \dot{X} without the second term in Eq. (113) with the dashed orange line. We also show the terminal velocity for a purely linear potential with the dashed cyan line.

As we can see from the figure, the relaxion reaches the terminal velocity around $t \simeq 1 \text{ GeV}^{-1}$. Soon after, the second term in Eq. (113) is turned on and the velocity of the relaxion starts to oscillate. Our stopping mechanism is expected to work around $t \sim 10^3 \text{ GeV}^{-1}$ and the linear potential approximation is good in this timescale. Note that the relaxion continues to roll in the figure since we do not take into account the Higgs field.

We give another possibility for the origin of the fast-rolling, which does not require a radiation dominated era before inflation. Suppose that the field value of the relaxion at the onset of the inflation is randomly distributed in space. Here, we assume that the potential of Eq. (113) has already been developed. Then, in some of the Hubble patches, we find a small region that takes the value of the relaxion in a different potential well. If the vacuum energy of the interior is higher than that of the exterior, such a region starts to contract and eventually collapses. At the point of collapse, the released energy is converted to the kinetic energy of the relaxion and the relaxion starts to roll down the potential.

Let us move on to cosmological history after the relaxation. As is discussed in [1], we need to reproduce the observed CMB fluctuations and reheat the SM particles safely. In our mechanism, the e -folds during the relaxation is estimated as

$$\mathcal{N}_e \gtrsim \frac{3H^2}{r\epsilon^2}, \quad (130)$$

which is about 10^5 with the parameter sets in the previous section. The observed CMB fluctuations can be compatible with such a number of e -folds if we consider, for example, new inflation. After the inflation, the maximal temperature should not be raised above $\sim 100 \text{ GeV}$, otherwise the relaxion would start to roll again. Thus, we need another well-separated sector, into which the potential energy of the inflaton is dumped. We do not go further in details since it falls out of the scope of this paper.

Finally, let us comment on baryogenesis. Although the upper bound on the maximal temperature is similar as in [1], the situation is worse because we can not use the sphalerons to generate the baryon asymmetry. There are several ways to generate it with a very low reheating temperature by using the decay of inflaton or heavy particles [63–66], or by using the oscillations of mesons or baryons [67–69].

X. CONCLUSION

In the original relaxion mechanism, quantum tunneling is essential for finding a sufficiently long-lived vacuum. However, it requires an unacceptably large number of e -folds and the inflation sector seems to be extremely fine-tuned.

We have shown that a fast-rolling relaxion can easily avoid the above problem without extending the original relaxion model. In our mechanism, we allow the relaxion to fly over the bumps and trigger the Higgs oscillation around the critical point. Then, the relaxion accidentally hits a bump and stops due to the immediate development of the Higgs VEV. After the EW scale is relaxed, the first selected vacuum need not decay if its lifetime is much longer than the age of the universe.

In our mechanism, the edge solution plays an important role. We have examined it in detail and obtained the relations among the amplitude of the Higgs oscillation, the Higgs mass, and the velocity of the relaxion. They offer not only a physical explanation of the solution but also a very effective way to search for viable parameters.

To keep our mechanism viable in field theory, we have discussed possible resonant particle production. In particular, the Higgs oscillation could produce too many particles and hence is dangerous. We discussed that it can be avoided by limiting the number of the Higgs oscillations to be $\mathcal{O}(10)$.

We have found an interesting and viable parameter region, where the relaxion has a mass of $\mathcal{O}(100 \text{ GeV})$ and mixes with the Higgs boson. The collider experiments have started to constrain the parameter region. The cut-off scale is around 20 TeV and the fine-tuning of the Higgs mass is reduced by 10^4 .

We have also discussed a more realistic model and cosmological history, where the relaxion resides in a compact field space and the origin of the fast-roll is explained naturally. Importantly, the model is realized without introducing a super-Planckian field space.

We think a higher cut-off is an interesting direction to explore. Unfortunately, such a region typically suffers from a large number of Higgs oscillations and the analysis becomes much more complicated. However, our mechanism is possibly compatible with particle production and such a region may be explored by using lattice calculations.

ACKNOWLEDGMENTS

M.S. is supported in part by a JSPS Research Fellowship for Young Scientists Grant Number 18J12023. Y.S. is supported in part by the Grant-in-Aid for Innovative Areas (16H06492). This work is also supported by MEXT KAKENHI Grant Nos. 15H05889 (M.I.), No. 16H03991(M.I.), No. 17H02878(M.I.), and No. 18H05542 (M.I.), and World Premier International Research Center Initiative (WPI Initiative), MEXT, Japan. M.I. thank UC Irvine for hospitality while we are finalizing this work.

Appendix A: Resonance strength

In this appendix, we give estimates of the Floquet exponents of the Mathieu equation following [70].

The Mathieu equation is defined as

$$\frac{d^2}{dz^2}u(z) + (A - 2q \cos(2z))u(z) = 0 , \quad (\text{A1})$$

with real A and q .

From the Floquet's theorem, there exist solutions that satisfy

$$u(z + \pi) = e^{i\pi\nu}u(z) . \quad (\text{A2})$$

Here, ν is a complex constant called the Floquet exponent. Such a function can be expanded with functions with periodicity π as

$$u(z) = e^{i\nu z} \sum_{n \in \mathbb{Z}} c_n e^{-2inz} , \quad (\text{A3})$$

where c_n 's are expansion coefficients.

In the following, we evaluate

$$\nu = \nu(A, q) , \quad (\text{A4})$$

using the Whittaker-Hill formula.

We first obtain relations among the expansion coefficients by substituting Eq. (A3) to Eq. (A1). We get

$$c_n + \xi_n(c_{n+1} + c_{n-1}) = 0 , \quad (\text{A5})$$

where

$$\xi_n = \frac{q}{(\nu - 2n)^2 - A} . \quad (\text{A6})$$

These relations can be expressed as

$$\Xi c = 0 , \quad (\text{A7})$$

where

$$c = (\dots, c_1, c_0, c_{-1}, \dots) , \quad (\text{A8})$$

$$\Xi = \begin{pmatrix} \ddots & & & & \\ & 1 & \xi_1 & 0 & \\ & \xi_0 & 1 & \xi_0 & \\ & 0 & \xi_{-1} & 1 & \\ & & & & \ddots \end{pmatrix} . \quad (\text{A9})$$

As shown in [70], $(\Xi - \mathbf{I})$ is of trace class. It ensures that $\det \Xi$ is finite and is independent of the choice of basis used in the evaluation of the determinant. In addition, it can be shown that Ξ is invertible if and only if

$$\det \Xi \neq 0 . \quad (\text{A10})$$

Next, we see the analytic structure of $\Delta(\nu) \equiv \det \Xi$. As can be seen from Ξ , $\Delta(\nu)$ has simple poles²⁰ at

$$\nu = 2n \pm \sqrt{A} , \quad (\text{A11})$$

and is analytic for other ν . Since $\Delta(\nu+2) = \Delta(\nu)$ and $\Delta(\nu) = \Delta(-\nu)$, it is enough to study

²⁰ For a special case, $A \in \mathbb{Z}$, two simple poles merges into a pole of order 2. The following discussion is also applicable to such a case.

strip $\text{Re}(\nu) \in [0, 1]$, where we have only one pole²¹ at

$$\nu = \min \left[\sqrt{A} \bmod 2, -\sqrt{A} \bmod 2 \right] . \quad (\text{A12})$$

We define a function,

$$\mathcal{D}(\nu) = \frac{1}{\cos(\pi\nu) - \cos(\pi\sqrt{A})} , \quad (\text{A13})$$

which has a pole at the same position in the strip and satisfies $\mathcal{D}(\nu + 2) = \mathcal{D}(\nu)$ and $\mathcal{D}(\nu) = \mathcal{D}(-\nu)$. Thus, for an appropriate constant, $C \neq 0$,

$$\Theta(\nu) = \Delta(\nu) - C\mathcal{D}(\nu) , \quad (\text{A14})$$

has no singularities for any $\nu \in \mathbb{C}$. Since $\Theta(\nu)$ is a bounded entire function, it must be a constant from the Liouville's theorem. Taking the limit of $\nu \rightarrow i\infty$, we have

$$\lim_{\nu \rightarrow i\infty} \mathcal{D}(\nu) = 0 , \quad (\text{A15})$$

$$\lim_{\nu \rightarrow i\infty} \Delta(\nu) = 1 , \quad (\text{A16})$$

since Ξ goes to the identity matrix. Thus, we get

$$\Theta(\nu) = 1 . \quad (\text{A17})$$

Using $\nu = 0$ as a reference point, we have

$$\Delta(\nu) = 1 + \frac{D(\nu)}{D(0)}(\Delta(0) - 1) , \quad (\text{A18})$$

for $A \neq 4\ell^2$ with $\ell \in \mathbb{Z}$. For Eq. (A7) to have a non-trivial solution, we need $\Delta(\nu) = 0$, which gives

$$\sin^2 \frac{\pi\nu}{2} = \Delta(0) \sin^2 \frac{\pi\sqrt{A}}{2} , \quad (\text{A19})$$

which is called the Whittaker-Hill formula. Notice that we can extend it to $A \in \mathbb{R}$.

²¹ When $A < 0$, we slightly tilt the strip so that only one pole is in one strip.

Next, we evaluate $\Delta(0)$. We define finite truncated determinants, Δ_p 's, as

$$\Delta_p = \begin{vmatrix} 1 & \bar{\xi}_p & & \\ \bar{\xi}_{p-1} & 1 & & \\ & & \ddots & \\ & & & 1 & \bar{\xi}_{p-1} \\ & & & \bar{\xi}_p & 1 \end{vmatrix}, \quad (\text{A20})$$

where $\bar{\xi}_n = \xi_n(\nu = 0) = \frac{q}{4n^2 - A}$. Then, we have

$$\Delta(0) = \lim_{p \rightarrow \infty} \Delta_p. \quad (\text{A21})$$

In the following, we obtain a recursion formula for Δ_p . The Laplace expansions for the first row give

$$\Delta_p = \Delta_p^{(-1)} - \alpha_p \Delta_p^{(-2)}, \quad (\text{A22})$$

where

$$\alpha_p = \bar{\xi}_p \bar{\xi}_{p-1}, \quad (\text{A23})$$

and $\Delta_p^{(-n)}$ is Δ_p without the first n columns and the first n rows. In the second term, we further developed the determinant along the first column.

Similarly, we have

$$\Delta_p^{(-1)} = \Delta_{p-1} - \alpha_p \Delta_{p-1}^{(-1)}, \quad (\text{A24})$$

$$\Delta_p^{(-2)} = \Delta_{p-1}^{(-1)} - \alpha_p \Delta_{p-2}. \quad (\text{A25})$$

After erasing $\Delta_p^{(-2)}$, we have

$$\Delta_p^{(-1)} + \alpha_p \Delta_{p-1}^{(-1)} = \Delta_{p-1}, \quad (\text{A26})$$

$$\Delta_p^{(-1)} - \alpha_p \Delta_{p-1}^{(-1)} = \Delta_p - \alpha_p^2 \Delta_{p-2}. \quad (\text{A27})$$

From these, we obtain

$$\Delta_p = (1 - \alpha_p) \Delta_{p-1} - \alpha_p (1 - \alpha_p) \Delta_{p-2} + \alpha_p \alpha_{p-1}^2 \Delta_{p-3}. \quad (\text{A28})$$

The first three terms are given by

$$\Delta_{-1} = 0, \quad \Delta_0 = 1, \quad \Delta_1 = 1 - 2\alpha_1. \quad (\text{A29})$$

Here, we defined Δ_{-1} so that it reproduces Δ_2 .

The leading terms in q^2 can be calculated as

$$\lim_{p \rightarrow \infty} \Delta_p = 1 - \frac{\pi \cot\left(\frac{\sqrt{A}}{2}\pi\right)}{4\sqrt{A}(A-1)} q^2 + \mathcal{O}(q^4). \quad (\text{A30})$$

It shows that instability of Eq. (A19) appears around $A = n^2$, $n \in \mathbb{Z}$ for a small q . The most important resonance bands are $A = 1$ and $A = 4$, which we call the first and the second resonance bands, respectively.

For a more precise determination of the Floquet exponents around these resonance bands, we solve Eq. (A28) up to a sufficiently large p . We get

$$\begin{aligned} (\nu - 1)^2 = & -\frac{1}{4}q^2 + \left(\frac{1}{4}(A-1)^2 + \frac{3}{16}(A-1)q^2 + \frac{15}{256}q^4 \right) \\ & - \left(\frac{1}{8}(A-1)^3 + \frac{5}{32}(A-1)^2q^2 + \frac{245}{3072}(A-1)q^4 + \frac{40}{2011}q^6 \right) \\ & + \mathcal{O}[(A-1, q^2)^4], \end{aligned} \quad (\text{A31})$$

$$\begin{aligned} (\nu - 2)^2 = & \left(\frac{1}{16}(A-4)^2 - \frac{1}{48}(A-4)q^2 - \frac{5}{2304}q^4 \right) \\ & + \left(-\frac{1}{128}(A-4)^3 + \frac{25}{2304}(A-4)^2q^2 + \frac{3}{3160}(A-4)q^4 + \frac{1}{94793}q^6 \right) \\ & + \mathcal{O}[(A-4, q^2)^4]. \end{aligned} \quad (\text{A32})$$

Here, the rational coefficients are determined by rationalizing numerical results with $p = 1000$.

Truncating them at $\mathcal{O}(q^4)$, we have

$$\nu|_{A \simeq 1} = 1 \pm \frac{i}{2} \sqrt{q^2 \left(1 - \frac{3}{32}q^2 \right) - \left(A - 1 + \frac{3}{8}q^2 \right)^2}, \quad (\text{A33})$$

$$\nu|_{A \simeq 4} = 2 \pm \frac{i}{4} \sqrt{\frac{1}{16}q^4 - \left(A - 4 - \frac{1}{6}q^2 \right)^2}. \quad (\text{A34})$$

Appendix B: Edge solution in the relaxion-Higgs system

In this appendix, we derive Eqs. (31) and (32).

We put an ansatz for the edge solution as

$$\bar{X}(t) = \frac{M^2 - m_\Phi^2}{\epsilon} + f\omega_X t + \varphi_0(t) , \quad (\text{B1})$$

$$\bar{h}(t) = \mathcal{A}_h \cos\left(\frac{\omega_X}{2}t - \alpha\right) + \chi_0(t) , \quad (\text{B2})$$

where φ_0 and χ_0 are functions and α , \mathcal{A}_h , m_Φ^2 and ω_X are constants. Here, we assume $|t| \ll |m_\Phi^2/(\epsilon f \omega_X)|$.

Substituting Eqs. (B1) and (B2) into Eqs. (11) and (12), we get

$$\begin{aligned} \ddot{\varphi}_0 + 3H\dot{\varphi}_0 = & \left[r\epsilon M^2 - 3fH\omega_X + \frac{\Lambda_h^2 \mathcal{A}_h^2}{8f} \sin 2\alpha \right] \\ & + \left[\frac{2\Lambda_0^4 + \Lambda_h^2 \mathcal{A}_h^2}{4f} \sin \omega_X t + \frac{\Lambda_h^2 \mathcal{A}_h^2}{8f} \sin(2\omega_X t - 2\alpha) \right] \\ & + \left[\frac{\Lambda_h^2 \mathcal{A}_h^2}{8f^2} \cos 2\alpha \right] \varphi_0 \\ & + \left[\frac{2\Lambda_0^4 + \Lambda_h^2 \mathcal{A}_h^2}{4f^2} \cos \omega_X t + \frac{\Lambda_h^2 \mathcal{A}_h^2}{8f^2} \cos(2\omega_X t - 2\alpha) \right] \varphi_0 \\ & + \frac{\Lambda_h^2 \mathcal{A}_h^2}{2f} \left[\sin\left(\frac{\omega_X}{2}t + \alpha\right) + \sin\left(\frac{3\omega_X}{2}t - \alpha\right) \right] \chi_0 , \end{aligned} \quad (\text{B3})$$

$$\begin{aligned} \ddot{\chi}_0 + 3H\dot{\chi}_0 = & \left[\frac{3H\omega_X \mathcal{A}_h}{2} \sin\left(\frac{\omega_X}{2}t - \alpha\right) - \frac{\Lambda_h^2 \mathcal{A}_h}{2} \cos\left(\frac{\omega_X}{2}t + \alpha\right) \right. \\ & \left. + \left(\frac{\omega_X^2 \mathcal{A}_h}{4} - m_\Phi^2 \mathcal{A}_h - \frac{3\lambda \mathcal{A}_h^3}{16} \right) \cos\left(\frac{\omega_X}{2}t - \alpha\right) \right] \\ & - \left[\frac{\Lambda_h^2 \mathcal{A}_h}{2} \cos\left(\frac{3\omega_X}{2}t - \alpha\right) + \frac{\lambda \mathcal{A}_h^3}{16} \cos\left(\frac{3\omega_X}{2}t - 3\alpha\right) \right] \\ & - \left[m_\Phi^2 + \frac{3\lambda \mathcal{A}_h^2}{8} \right] \chi_0 \\ & - \left[\Lambda_h^2 \cos \omega_X t + \frac{3\lambda \mathcal{A}_h^2}{8} \cos(\omega_X t - 2\alpha) \right] \chi_0 \\ & + \frac{\Lambda_h^2 \mathcal{A}_h}{2f} \left[\sin\left(\frac{\omega_X}{2}t + \alpha\right) + \sin\left(\frac{3\omega_X}{2}t - \alpha\right) \right] \varphi_0 . \end{aligned} \quad (\text{B4})$$

Here, we changed the overall phase so that $\cos[(M^2 - m_\Phi^2)/(\epsilon f)] = 1$. We have ignored the

other non-linear terms and the terms with ϵ unless multiplied by M^2 .

In the following, we search for a special solution that is expressed as

$$\chi_0(t) = \sum_{p=1}^{\infty} c_p^{\chi} \cos \left[\left(p + \frac{1}{2} \right) \omega_X t + \alpha_p \right] , \quad (\text{B5})$$

$$\varphi_0(t) = \sum_{p=1}^{\infty} c_p^{\varphi} \cos (p\omega_X t + \beta_p) , \quad (\text{B6})$$

where $c_p^{\chi}, c_p^{\varphi}, \alpha_p$ and β_p are constants. Notice that we can always choose \mathcal{A}_h and α so that χ_0 does not contain the mode with $p = 0$.

Integrating Eq. (B4) over t multiplying $\sin(\omega_X t/2 - \alpha)$ or $\cos(\omega_X t/2 - \alpha)$, we have

$$\begin{aligned} \sin 2\alpha &= -\frac{3H\omega_X}{\Lambda_h^2} - \frac{c_1^{\chi}}{\mathcal{A}_h} \left[\sin(\alpha + \alpha_1) + \frac{3\mathcal{A}_h^2}{8\Lambda_h^2} \sin(3\alpha + \alpha_1) \right] \\ &\quad + \frac{c_2^{\varphi}}{2f} \cos(2\alpha + \beta_2) , \end{aligned} \quad (\text{B7})$$

$$\begin{aligned} m_{\Phi}^2 + \frac{3\lambda}{16} \mathcal{A}_h^2 &= \frac{\omega_X^2}{4} - \frac{\Lambda_h^2}{2} \cos 2\alpha \\ &\quad - \frac{c_1^{\chi}}{\mathcal{A}_h} \left[\frac{\Lambda_h^2}{2} \cos(\alpha + \alpha_1) + \frac{3\lambda\mathcal{A}_h^2}{16} \cos(3\alpha + \alpha_1) \right] \\ &\quad - \frac{c_1^{\varphi}}{2f} \Lambda_h^2 \sin \beta_1 - \frac{c_2^{\varphi}}{2f} \frac{\Lambda_h^2}{2} \sin(2\alpha + \beta_2) . \end{aligned} \quad (\text{B8})$$

Similarly, by integrating Eq. (B3) over t , we have

$$\begin{aligned} \omega_X &= \frac{r\epsilon M^2}{3fH} + \frac{\Lambda_h^2 \mathcal{A}_h^2}{24Hf^2} \sin 2\alpha \\ &\quad + \frac{c_1^{\varphi}}{2f} \frac{2\Lambda_0^4 + \Lambda_h^2 \mathcal{A}_h^2}{12Hf^2} \cos \beta_1 + \frac{c_2^{\varphi}}{2f} \frac{\Lambda_h^2 \mathcal{A}_h^2}{24Hf^2} \cos(2\alpha + \beta_2) \\ &\quad - \frac{c_1^{\chi}}{\mathcal{A}_h} \frac{\Lambda_h^2 \mathcal{A}_h^2}{12Hf^2} \sin(\alpha + \alpha_1) . \end{aligned} \quad (\text{B9})$$

Comparing the results with (27), we find²² $\cos 2\alpha < 0$ and we obtain

$$\alpha \simeq \pm \frac{\pi}{2} + \frac{3H\omega_X}{2\Lambda_h^2} , \quad (\text{B10})$$

assuming c_1^{χ} and c_2^{φ} are small. Notice that we do not have the edge solution when $\frac{3H\omega_X}{\Lambda_h^2} \gtrsim 1$, where the resonance of the Higgs field does not occur due to a large

²² The other possibility corresponds to the other edge of the resonance band.

Hubble friction.

Repeating similar calculations multiplying sines and cosines with other frequencies, we get

$$\alpha_1 \simeq \pm \frac{\pi}{2} - 3H \left(\frac{\omega_X}{2\Lambda_h^2} \frac{3\lambda\mathcal{A}_h^2 - 8\Lambda_h^2}{\lambda\mathcal{A}_h^2 - 8\Lambda_h^2} + \frac{6\omega_X}{4m_\Phi^2 - 9\omega_X^2} \right), \quad (\text{B11})$$

$$\beta_1 \simeq \pm \frac{\pi}{2} + \frac{3H}{16f^2\omega_X} (\mathcal{A}_h^2 + 16f^2), \quad (\text{B12})$$

$$\beta_2 \simeq \pm \frac{\pi}{2} - 3H \left(\frac{\omega_X}{\Lambda_h^2} - \frac{1}{2\omega_X} \right), \quad (\text{B13})$$

and

$$c_1^X \simeq -\text{sign}(\alpha\alpha_1) \frac{8\Lambda_h^2 - \lambda\mathcal{A}_h^2}{4(9\omega_X^2 - 4m_\Phi^2)} \mathcal{A}_h \left(1 + \frac{18\lambda\mathcal{A}_h^2\omega_X^2(18\omega_X^2 + 3\lambda\mathcal{A}_h^2 - 8m_\Phi^2)}{\Lambda_h^2(8\Lambda_h^2 - \lambda\mathcal{A}_h^2)^2(9\omega_X^2 - 4m_\Phi^2)} H^2 \right), \quad (\text{B14})$$

$$c_1^\varphi \simeq \text{sign}(\beta_1) \frac{2\Lambda_0^4 + \Lambda_h^2\mathcal{A}_h^2}{4f^2\omega_X^2} f \left(1 - \frac{9\mathcal{A}_h^2}{32f^2\Lambda_h^2} H^2 \right), \quad (\text{B15})$$

$$c_2^\varphi \simeq -\text{sign}(\beta_2) \frac{\Lambda_h^2\mathcal{A}_h^2}{32f^2\omega_X^2} f \left(1 - \frac{9\mathcal{A}_h^2}{64f^2\Lambda_h^2} H^2 \right). \quad (\text{B16})$$

Here, we have ignored $\mathcal{O}(1/\omega_X^3)$, $\mathcal{O}(H^2/\omega_X)$ and $\mathcal{O}(H^3)$ corrections. Plugging them into Eqs. (B8) and (B9), we obtain²³ Eqs. (31) and (32).

Appendix C: Another mechanism to stop the relaxion

Here, we present another mechanism to stop the relaxion without slow-roll. It is summarized below.

1. The initial Higgs mass is assumed to be positive and the relaxion rolls down the potential with its terminal velocity.
- 2' The relaxion go through the critical point without suffering from any resonance and the Higgs field develops a VEV.
- 3' The height of the bumps increases as the Higgs VEV increases. It enhances the difference between the maximum and the minimum velocities of the relaxion.

²³ The signs of α_1, β_1 and β_2 do not affect the result.

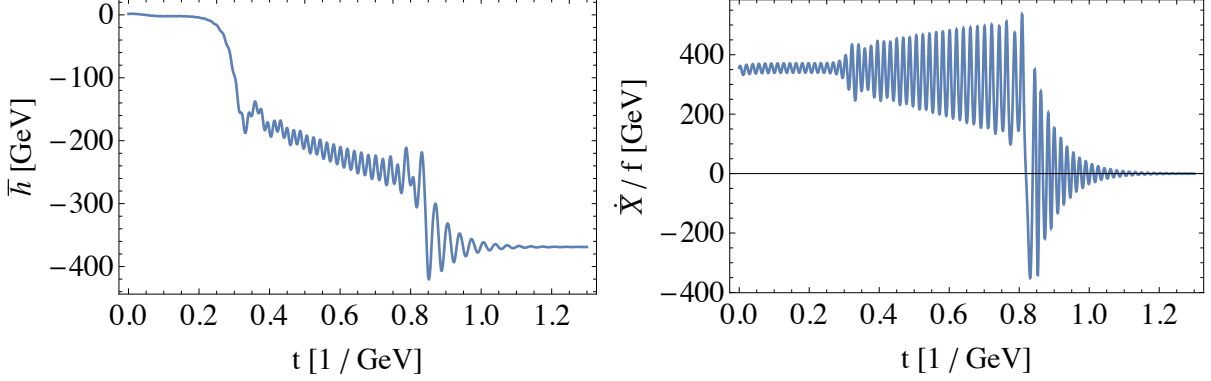


FIG. 12. Another stopping mechanism. The left and the right panels show the evolution of \bar{h} and \dot{X}/f , respectively.

4' The minimum velocity of the relaxion reaches zero and the relaxion gets trapped between bumps.

5' The kinetic energy of the Higgs field and the relaxion dumps quickly by the Hubble friction.

We show an example in Fig. 12. The left and the right panels show the evolution of \bar{h} and \dot{X}/f , respectively. We take

$$\begin{aligned} \lambda &= 0.52, \quad H = 10 \text{ GeV}, \quad \Lambda_0 = \Lambda_h = 80 \text{ GeV}, \quad \epsilon = 0.8 \text{ GeV}, \quad r = 0.002, \\ f &= 60 \text{ GeV}, \quad M = 20 \text{ TeV}. \end{aligned} \tag{C1}$$

The Higgs mass becomes negative around $t \simeq 0.1$. After $t \simeq 0.2$, the Higgs field develops a VEV and the range of the relaxion velocity spreads out. The minimum of the velocity reaches zero at $t \sim 0.8$ and the relaxion gets trapped.

With this example point, one can show that the resonant particle production is very efficient after the Higgs field obtains a VEV. Thus, it is preferable to stop the relaxion just after the Higgs field obtains a VEV. Such an example point is Point 3 of Fig. 9.

-
- [1] P. W. Graham, D. E. Kaplan, and S. Rajendran, Phys. Rev. Lett. **115**, 221801 (2015), arXiv:1504.07551 [hep-ph].
- [2] R. S. Gupta, J. Y. Reiness, and M. Spannowsky, (2019), arXiv:1902.08633 [hep-ph].

- [3] A. Banerjee, D. Budker, J. Eby, H. Kim, and G. Perez, (2019), arXiv:1902.08212 [hep-ph].
- [4] S.-J. Wang, (2018), arXiv:1811.06520 [hep-ph].
- [5] A. Hook and G. Marques-Tavares, JHEP **12**, 101 (2016), arXiv:1607.01786 [hep-ph].
- [6] K. Choi and S. H. Im, JHEP **12**, 093 (2016), arXiv:1610.00680 [hep-ph].
- [7] N. Fonseca, E. Morgante, and G. Servant, JHEP **10**, 020 (2018), arXiv:1805.04543 [hep-ph].
- [8] W. Tangarife, K. Tobioka, L. Ubaldi, and T. Volansky, (2017), arXiv:1706.00438 [hep-ph].
- [9] K. Choi, H. Kim, and T. Sekiguchi, Phys. Rev. **D95**, 075008 (2017), arXiv:1611.08569 [hep-ph].
- [10] W. Tangarife, K. Tobioka, L. Ubaldi, and T. Volansky, JHEP **02**, 084 (2018), arXiv:1706.03072 [hep-ph].
- [11] O. Matsedonskyi and M. Montull, Phys. Rev. **D98**, 015026 (2018), arXiv:1709.09090 [hep-ph].
- [12] S. A. Abel, R. S. Gupta, and J. Scholtz, (2018), arXiv:1810.05153 [hep-ph].
- [13] A. Banerjee, H. Kim, and G. Perez, (2018), arXiv:1810.01889 [hep-ph].
- [14] M. Geller, Y. Hochberg, and E. Kuflik, (2018), arXiv:1809.07338 [hep-ph].
- [15] N. Fonseca and E. Morgante, (2018), arXiv:1809.04534 [hep-ph].
- [16] C. Frugiuele, E. Fuchs, G. Perez, and M. Schlaffer, JHEP **10**, 151 (2018), arXiv:1807.10842 [hep-ph].
- [17] O. Davidi, R. S. Gupta, G. Perez, D. Redigolo, and A. Shalit, JHEP **08**, 153 (2018), arXiv:1806.08791 [hep-ph].
- [18] R. S. Gupta, Phys. Rev. **D98**, 055023 (2018), arXiv:1805.09316 [hep-ph].
- [19] N. Fonseca, B. Von Harling, L. De Lima, and C. S. Machado, JHEP **07**, 033 (2018), arXiv:1712.07635 [hep-ph].
- [20] K. S. Jeong and C. S. Shin, JHEP **01**, 121 (2018), arXiv:1709.10025 [hep-ph].
- [21] A. Nelson and C. Prescod-Weinstein, Phys. Rev. **D96**, 113007 (2017), arXiv:1708.00010 [hep-ph].
- [22] B. Batell, M. A. Fedderke, and L.-T. Wang, JHEP **12**, 139 (2017), arXiv:1705.09666 [hep-ph].
- [23] T. You, JCAP **1709**, 019 (2017), arXiv:1701.09167 [hep-ph].
- [24] Z. Lalak and A. Markiewicz, J. Phys. **G45**, 035002 (2018), arXiv:1612.09128 [hep-ph].
- [25] L. McAllister, P. Schwaller, G. Servant, J. Stout, and A. Westphal, JHEP **02**, 124 (2018), arXiv:1610.05320 [hep-th].
- [26] T. Flacke, C. Frugiuele, E. Fuchs, R. S. Gupta, and G. Perez, JHEP **06**, 050 (2017),

- arXiv:1610.02025 [hep-ph].
- [27] T. Kobayashi, O. Seto, T. Shimomura, and Y. Urakawa, *Mod. Phys. Lett.* **A32**, 1750142 (2017), arXiv:1605.06908 [astro-ph.CO].
 - [28] J. L. Evans, T. Gherghetta, N. Nagata, and Z. Thomas, *JHEP* **09**, 150 (2016), arXiv:1602.04812 [hep-ph].
 - [29] A. Fowlie, C. Balazs, G. White, L. Marzola, and M. Raidal, *JHEP* **08**, 100 (2016), arXiv:1602.03889 [hep-ph].
 - [30] L. E. Ibanez, M. Montero, A. Uranga, and I. Valenzuela, *JHEP* **04**, 020 (2016), arXiv:1512.00025 [hep-th].
 - [31] S. Di Chiara, K. Kannike, L. Marzola, A. Racioppi, M. Raidal, and C. Spethmann, *Phys. Rev.* **D93**, 103527 (2016), arXiv:1511.02858 [hep-ph].
 - [32] L. Marzola and M. Raidal, *Mod. Phys. Lett.* **A31**, 1650215 (2016), arXiv:1510.00710 [hep-ph].
 - [33] R. S. Gupta, Z. Komargodski, G. Perez, and L. Ubaldi, *JHEP* **02**, 166 (2016), arXiv:1509.00047 [hep-ph].
 - [34] J. Jaeckel, V. M. Mehta, and L. T. Witkowski, *Phys. Rev.* **D93**, 063522 (2016), arXiv:1508.03321 [hep-ph].
 - [35] O. Antipin and M. Redi, *JHEP* **12**, 031 (2015), arXiv:1508.01112 [hep-ph].
 - [36] S. P. Patil and P. Schwaller, *JHEP* **02**, 077 (2016), arXiv:1507.08649 [hep-ph].
 - [37] E. Hardy, *JHEP* **11**, 077 (2015), arXiv:1507.07525 [hep-ph].
 - [38] A. Kobakhidze, *Eur. Phys. J.* **C75**, 384 (2015), arXiv:1506.04840 [hep-ph].
 - [39] S. Iso, K. Kohri, and K. Shimada, *Phys. Rev.* **D93**, 084009 (2016), arXiv:1511.05923 [hep-ph].
 - [40] M. Dine and L. Pack, *JCAP* **1206**, 033 (2012), arXiv:1109.2079 [hep-ph].
 - [41] G. German, G. G. Ross, and S. Sarkar, *Nucl. Phys.* **B608**, 423 (2001), arXiv:hep-ph/0103243 [hep-ph].
 - [42] H. Beauchesne, E. Bertuzzo, and G. Grilli di Cortona, *JHEP* **08**, 093 (2017), arXiv:1705.06325 [hep-ph].
 - [43] H. Matsui and F. Takahashi, *Phys. Rev.* **D99**, 023533 (2019), arXiv:1807.11938 [hep-th].
 - [44] K. Dimopoulos, *Phys. Rev.* **D98**, 123516 (2018), arXiv:1810.03438 [gr-qc].
 - [45] W. H. Kinney, *Phys. Rev. Lett.* **122**, 081302 (2019), arXiv:1811.11698 [astro-ph.CO].
 - [46] R. Allahverdi, R. Brandenberger, F.-Y. Cyr-Racine, and A. Mazumdar, *Ann. Rev. Nucl. Part. Sci.* **60**, 27 (2010), arXiv:1001.2600 [hep-th].

- [47] S. R. Coleman, Phys. Rev. **D15**, 2929 (1977), [Erratum: Phys. Rev.D16,1248(1977)].
- [48] C. G. Callan, Jr. and S. R. Coleman, Phys. Rev. **D16**, 1762 (1977).
- [49] P. Bechtle, O. Brein, S. Heinemeyer, O. Stl, T. Stefaniak, G. Weiglein, and K. E. Williams, Eur. Phys. J. **C74**, 2693 (2014), arXiv:1311.0055 [hep-ph].
- [50] P. Bechtle, O. Brein, S. Heinemeyer, O. Stal, T. Stefaniak, G. Weiglein, and K. Williams, *Proceedings, 4th International Workshop on Prospects for Charged Higgs Discovery at Colliders (CHARGED 2012): Uppsala, Sweden, October 8-11, 2012*, PoS **CHARGED2012**, 024 (2012), arXiv:1301.2345 [hep-ph].
- [51] P. Bechtle, O. Brein, S. Heinemeyer, G. Weiglein, and K. E. Williams, Comput. Phys. Commun. **182**, 2605 (2011), arXiv:1102.1898 [hep-ph].
- [52] P. Bechtle, O. Brein, S. Heinemeyer, G. Weiglein, and K. E. Williams, Comput. Phys. Commun. **181**, 138 (2010), arXiv:0811.4169 [hep-ph].
- [53] P. Bechtle, S. Heinemeyer, O. Stal, T. Stefaniak, and G. Weiglein, Eur. Phys. J. **C75**, 421 (2015), arXiv:1507.06706 [hep-ph].
- [54] P. Bechtle, S. Heinemeyer, O. Stl, T. Stefaniak, and G. Weiglein, JHEP **11**, 039 (2014), arXiv:1403.1582 [hep-ph].
- [55] P. Bechtle, S. Heinemeyer, O. Stl, T. Stefaniak, and G. Weiglein, Eur. Phys. J. **C74**, 2711 (2014), arXiv:1305.1933 [hep-ph].
- [56] The ATLAS collaboration, .
- [57] CMS Collaboration, .
- [58] G. F. Giudice and M. McCullough, JHEP **02**, 036 (2017), arXiv:1610.07962 [hep-ph].
- [59] D. E. Kaplan and R. Rattazzi, Phys. Rev. **D93**, 085007 (2016), arXiv:1511.01827 [hep-ph].
- [60] K. Choi and S. H. Im, JHEP **01**, 149 (2016), arXiv:1511.00132 [hep-ph].
- [61] K. Harigaya and M. Ibe, Phys. Lett. **B738**, 301 (2014), arXiv:1404.3511 [hep-ph]; JHEP **11**, 147 (2014), arXiv:1407.4893 [hep-ph].
- [62] R. Coy, M. Frigerio, and M. Ibe, JHEP **10**, 002 (2017), arXiv:1706.04529 [hep-ph].
- [63] R. J. Scherrer, J. M. Cline, S. Raby, and D. Seckel, Phys. Rev. **D44**, 3760 (1991).
- [64] A. Pierce and B. Shakya, (2019), arXiv:1901.05493 [hep-ph].
- [65] S. Dimopoulos and L. J. Hall, Phys. Lett. **B196**, 135 (1987).
- [66] K. S. Babu, R. N. Mohapatra, and S. Nasri, Phys. Rev. Lett. **97**, 131301 (2006), arXiv:hep-ph/0606144 [hep-ph].

- [67] A. E. Nelson and H. Xiao, (2019), arXiv:1901.08141 [hep-ph].
- [68] K. Aitken, D. McKeen, T. Neder, and A. E. Nelson, Phys. Rev. **D96**, 075009 (2017), arXiv:1708.01259 [hep-ph].
- [69] G. Elor, M. Escudero, and A. Nelson, Phys. Rev. **D99**, 035031 (2019), arXiv:1810.00880 [hep-ph].
- [70] J. E. Sträng, Acad. Roy. Belg. Bull. Cl. Sci. (6) 16 (2005), no. 7-12, 269–287.